A potent inhibitor of PAI-1, MDI-2517, mitigates disease severity in a preclinical systemic sclerosis model

Enming J. Su[1], Pei-Suen Tsou[2], Mark Warnock[1], Natalya Subbotina[3], Kris Mann[1], Sirapa Vichaikul[2], Alyssa Rosek[2], Lisa Leung[4], Xianying Xing[5], Enze Xing[5], Olesya Plazyo[5], Rachael Bogle[5], Lam C. Tsoi[5], Cory D. Emal[6], Dinesh Khanna[2], John Varga[2], Thomas H. Sisson[3], Johann E Gudjonsson[2,5], Daniel A. Lawrence[1]*

[1] Division of Cardiovascular Medicine, Department of Internal Medicine, University of Michigan Medical School, Ann Arbor, Michigan, USA.

[2] Scleroderma Program, Division of Rheumatology, Department of Internal Medicine, University of Michigan Medical School, Ann Arbor, Michigan, USA.

[3] Division of Pulmonary and Critical Care Medicine, Department of Internal Medicine, University of Michigan, Ann Arbor, Michigan, USA.

[4] Department of Molecular Integrative Physiology, University of Michigan, Ann Arbor, Michigan, USA.

[5] Department of Dermatology, University of Michigan, Ann Arbor, MI, USA.

[5] Department of Chemistry, Eastern Michigan University, Ypsilanti, MI, USA.

*Address correspondence to: Daniel Lawrence, 7301 MSRB III, 1150 W. Medical Center Dr., Ann Arbor MI 48109-0644., Tel.: Phone: 734-936-9549; Fax: 734-936-2641; E-mail: dlawrenc@umich.edu.

Key Words: PAI-1, MDI-2517, Fibrosis, Scleroderma, Interstitial-Lung-Disease

Conflict-of-interest statement: EJS, CDE, DK, and DAL hold interest in MDI Therapeutics which has a license from the University of Michigan for MDI-2517. DAL, DK, and JV are members of the MDI Therapeutics Clinical & Science Advisory Board. DAL, CDE, and MW are inventors on patents for MDI-2517, US 9,718,760-B2, US 11,426,368-B2, and US 12,390,427-B2. DK has served as a consultant to Amgen, Abbvie, Astra Zeneca, Boehringer Ingelheim, BMS, GSK, and Zura Bio. JEG has received research grants from Eli Lilly, Almirall, BMS, Prometheus/Merck, Boehringer Ingelheim, Novartis, Janssen, and AbbVie and has served as an advisor to Eli Lilly, Takeda, BMS, Novartis, Almirall, Janssen, Sanofi, AbbVie, MDI-Therapeutics, and Boehringer Ingelheim. All other authors have declared that no conflict of interest exists.

Abstract

Systemic sclerosis (SSc) is a complex and heterogeneous condition characterized by progressive fibrosis in multiple organs. Recent studies implicate plasminogen activator inhibitor 1 (PAI-1) in the pathogenesis of SSc, and PAI-1 is considered as a potential target for therapy. Here, using single-cell and spatial RNA-seq analysis of skin biopsies from 18 healthy individuals and 22 SSc patients, we found elevated PAI-1 co-localizing to myofibroblasts with enriched extracellular matrix-associated biological processes. Treatment of SSc dermal fibroblasts with the small molecule PAI-1 inhibitor MDI-2517 reduced the expression of the profibrotic markers *COL1A1* and *ACTA2*. To investigate the therapeutic potential of MDI-2517, we evaluated its efficacy in reducing fibrosis in a preclinical model of SSc. Treatment of mice with MDI-2517 significantly reduced both skin and lung fibrosis and was superior to treatment with either pirfenidone or mycophenolate mofetil. Additionally, MDI-2517 attenuated weight loss and significantly reduced the expression of key profibrotic markers. Compared to tiplaxtinin, another PAI-1 inhibitor previously shown to be effective in a model of SSc, MDI-2517 was found to have superior efficacy at a 10-fold lower dose. These findings highlight the role of PAI-1 in the pathogenesis of SSc, and the potential of MDI-2517 for the treatment of SSc.

Introduction

Systemic sclerosis (SSc), also called scleroderma, is a chronic autoimmune disorder characterized by fibrosis (thickening and hardening) of the skin, blood vessels, and internal organs. This condition primarily affects the connective tissue, resulting in widespread inflammation and the overproduction of collagen (1, 2). SSc is associated with a range of symptoms, including skin tightening, joint pain, organ dysfunction, and vascular complications. Clinically progressive interstitial lung disease (ILD) occurs in approximately 40% of SSc cases and is the leading cause of death in SSc (3-7). There is no known cure for SSc, and current treatments aim to manage symptoms, slow disease progression, and improve quality of life (8). Treatment options involve a combination of pharmacological and non-pharmacological interventions. Pharmacotherapies focus on controlling inflammation, alleviating symptoms, and targeting specific manifestations of the disease. Immunosuppressive medications, such as methotrexate, mycophenolate mofetil (MMF), and cyclophosphamide, are used to modulate the immune response and reduce inflammation (9). For the treatment of SSc-ILD, the two approved therapies, nintedanib, and tocilizumab, only slow, but do not stop or reverse the decline in pulmonary function (10).

In recent years, targeted therapies have shown promise in managing SSc. Studies have identified potential molecular targets and pathways that play a crucial role in the pathogenesis of the disease. One such target is plasminogen activator inhibitor-1 (PAI-1), a protein involved in the regulation of fibrinolysis, extracellular matrix remodeling, and wound healing (11-15). PAI-1, encoded by the *SERPINE1* gene, is elevated in SSc patients, and is thought to contribute to the excessive accumulation of collagen, leading to tissue fibrosis (16, 17). PAI-1 serves as the physiological inhibitor of tissue and urokinase plasminogen activator (tPA and uPA). Under physiological conditions, PAI-1 plays an important role in regulating fibrinolysis and wound healing. However, excessive PAI-1 activity has been strongly associated with fibrotic diseases,

including pulmonary fibrosis. Animal models of pulmonary fibrosis have indicated that inhibiting PAI-1 could be an effective therapeutic strategy for this debilitating condition (18, 19).

In models of SSc, two preclinical studies have targeted PAI-1 with either the small molecule tiplaxtinin (20), or with a monoclonal antibody to PAI-1 (11), and both showed reductions in skin fibrosis. In another study using transgenic mice over-expressing the transcription factor Snail in keratinocytes, the mice developed an SSc-like phenotype that was largely normalized by systemic PAI-1 deficiency (21). Together, these studies suggest that PAI-1 is an important mediator of fibrosis development in SSc. MDI-2517 is a more effective analog of a new class of small molecule inhibitors targeting PAI-1 (22), with a unique mechanism of action, and is currently in phase 1 clinical testing (NCT06453824). MDI-2517 offers the potential of an anti-fibrotic treatment by moderating the activity of PAI-1, which contributes to the pathogenesis of SSc. In the studies presented here, we sought to evaluate PAI-1 expression in patients with SSc and to assess MDI-2517 in a model of SSc for efficacy to reduce fibrogenic progression, collagen accumulation, and overall disease severity in both skin and lung. Our results provide important insight into the therapeutic potential of MDI-2517 for the treatment of SSc with ILD.

Results

Expression of PAI-1 in human SSc skin samples.

Comparison of *SERPINE1* expression in skin biopsies from 36 normal individuals with 66 SSc patients from the GEO dataset (GSE58095) demonstrated a significant increase in *SERPINE1* expression in the patient skin that was strongly correlated with their modified Rodnan skin score (**Figure 1 A** and **B**). We next utilized single-cell RNA-seq analyses of skin biopsies from 18 healthy controls and 22 SSc patients along with spatial-sequencing of lesional SSc skin from 4 subjects that we have previously published (23) to assess *SERPINE1* expression. We observed a marked overlap in the expression of *SERPINE1* and genes involved in extracellular matrix remodeling and myofibroblast phenotype (as defined by *COL8A1* expression) (**Figure 1C** and supplemental **Figure S1**). This finding was verified by identifying increased *SERPINE1* expression in cell types obtained from lesional SSc versus healthy control skin. Specifically, we found upregulated expression of *SERPINE1* in SSc fibroblasts, and, to a lesser extent, in SSc endothelial cells and keratinocytes relative to their control counterparts (**Figure 1D, upper panel**). When assessed across fibroblast subsets, the most prominent expression of *SERPINE1* was observed in *COL8A1* myofibroblasts (**Figure 1D, lower panel**). We further compared enriched biological processes (Reactome) in *SERPINE1*+ vs. *SERPINE1*- myofibroblasts and identified an enrichment of biological processes related to extracellular matrix, including extracellular matrix organization, collagen formation, and assembly of collagen fibrils (**Figure 1E)** (see Supplemental **Table S1** for the Gene components of our ECM module score). The presence of PAI-1 protein in SSc skin was validated by immunohistochemistry whereas little PAI-1 staining is observed in skin from a healthy control (**Figure 1F** and **G**).

Downregulation of pro-fibrotic biomarkers by PAI-1 inhibition in isolated SSc skin fibroblasts.

Consistent with the single cell sequencing data above, we found that in dermal fibroblasts collected from diffuse cutaneous (dc)SSc patients, there was a significant increase in PAI-1 expression compared to expression in dermal fibroblasts from healthy volunteers (**Figure 2A**). To examine the potential anti-fibrotic action of PAI-1 inhibition in SSc dermal fibroblasts, we measured gene expression of the fibrotic biomarkers smooth muscle actin (αSMA; gene *ACTA2*), and collagen 1A1 (gene *COL1A1*) with and without MDI-2517 treatment. We also examined the effect of MDI-2517 on the expression of *SERPINE1*. These data demonstrated that MDI-2517 treatment induced an approximate 50% reduction in both *ACTA2* and *COL1A1* expression compared to vehicle treated cells but did not inhibit *SERPINE1* expression (**Figure 2B** and supplementary **Figure S2**). The lack of a direct inhibition of *SERPINE1* expression is consistent with the known mechanism of action of this class of PAI-1 inhibitors that act directly on PAI-1 protein to inhibit its function but have not been shown to affect its expression (22). The reduction in the fibrotic response without reducing PAI-1 expression was further confirmed by immunoblotting for the protein products αSMA, COL1, and PAI-1 in SSc dermal fibroblasts treated with or without MDI-2517 (**Figure 2C** and **D**).

Oral administration of MDI-2517 reduces PAI-1 in skin, and systemic PAI-1 activity

Subcutaneous bleomycin administration to induce fibrosis is commonly used as a model of SSc in preclinical studies to evaluate the efficacy of antifibrotic treatments (24). For our studies bleomycin (100U/kg) was administered subcutaneously via an osmotic pump over a period of 7 days to induce systemic fibrosis. After 7 days, the pumps were removed, and animals were then placed on control chow or chow containing MDI-2517 (500 mg of MDI-2517/kg of chow) for an additional 3 weeks. This formulation was based on a preliminary dose finding study indicating that 500mg of MDI-2517 per kg of chow was a maximally effective dose at reducing skin thickening (supplemental **Figure S3**). Based on the average consumption of 10 to 15 grams of

chow per day per 100 grams of body weight for mice (25), this drug concentration is expected to result in an approximate daily dose of MDI-2517 of 60 mg/kg. Following this treatment we examined target engagement by MDI-2517 in both skin and plasma. PAI-1 protein in skin, and systemic PAI-1 antigen and activity in plasma were quantified on day 28. PAI-1 protein levels in skin were determined by immunofluorescent staining (**Figures 3A and 3B**) and PAI-1 antigen and activity in plasma were analyzed by a multiplex Luminex assay as described (26) (**Figure 3C**). Similar to human skin from a healthy control (**Figure 1G**), naïve mouse skin displayed little PAI-1 immunofluorescence (Supplemental **Figure S4**). In contrast, there was notable PAI-1 protein in mouse skin following bleomycin exposure that was significantly reduced by approximately 65% in MDI-2517-treated mice compared to vehicle treatment (**Figures 3A** and **B**). Likewise, the activity of PAI-1 in plasma showed a similar 56% reduction in MDI-2517 treated animals, while total PAI-1 antigen showed a non-significant reduction (**Figure 3C**).

MDI-2517 treatment is more efficacious than pirfenidone or Mycophenolate Mofetil (MMF) at reducing bleomycin-induced skin fibrosis in the Bleomycin Model of SSc

To compare the therapeutic efficacy of MDI-2517 to clinically administered anti-fibrotic and immunosuppressive drugs, including the current first-line standard of care MMF (27), systemic fibrosis was induced with bleomycin as above and the mice were placed on chow containing either MDI-2517 (500 mg/kg of chow) or MMF (1000 mg/kg of chow) or on chow containing pirfenidone (1000 mg/kg of chow). Pirfenidone is approved for the treatment of idiopathic pulmonary fibrosis and has been investigated in clinical trials for SSc (28). Compared to either MMF or pirfenidone, MDI-2517 showed superior efficacy in reducing skin thickness with over 50% reduction compared to vehicle control. In contrast, MMF treatment reduced skin thickness by approximately 15% ($p = 0.057$) while pirfenidone had no effect (**Figure 4A**). Further, both MDI-2517 and MMF-treated animals showed attenuated weight loss compared to vehicle or

pirfenidone treatment (**Figure 4B**). Known biomarkers of SSc were also examined, and these data demonstrated that MDI 2517 treatment reduces key biomarkers associated with disease progress in SSc patients. (**Figure 4C-E**). The biomarkers examined were serum surfactant protein-D (SP-D), a marker associated with the decline of forced vital capacity; Intercellular Adhesion Molecule 1 (ICAM-1), a marker known for regulating leukocyte recruitment from circulation to sites of inflammation; and MMP-9, a marker of fibrogenic remodeling during the progression of skin sclerosis in SSc. MDI-2517 showed superior efficacy in reducing all three biomarkers (SP-D, ICAM-1, and MMP-9) compared to pirfenidone and was superior to MMF in reducing MMP-9 (**Figure 4C-E**).

Comparator Study of MDI-2517 and MDI-2517+MMF combination in the Bleomycin Model of SSc

Since MMF is the standard of care for SSc patients, we examined if MDI-2517 would have benefit in combination with MMF in attenuating bleomycin induce skin fibrosis. As a control, pumps filled with saline were also implanted in two separate cohorts; one cohort was treated with control chow and another with chow containing MDI-2517 (500 mg/kg of chow). Compared to MMF alone or the control group, treatment with MDI-2517 or a combination of MDI-2517+MMF showed superior efficacy in reducing skin thickness with approximately 50% reduction compared to control chow, and similar to the results above, MMF alone resulted in a non-significant 16% reduction in skin thickness (**Figure 5A**). Additionally, MDI-2517 treated animals showed better attenuation in weight loss compared to vehicle and MMF-treated animals (**Figure 5B**). MDI-2517 treatment in the absence of the bleomycin insult did not affect dermal thickness or weight (**Figure 5A** and **B**).

To confirm skin thickness results measured by the pinch method, skin samples were processed and stained with Mason Trichrome (**Figure 6**). **Figures 6A** and **B** show the dermal layer of animals that received saline pumps and were treated with control chow or chow-

containing MDI-2517, respectively. Compared to these control conditions, animals receiving bleomycin pumps and treated with control chow had a much thicker dermal layer (**Figure 6C**), whereas MDI-2517 treated skin samples showed substantially less collagen deposition and a significantly thinner dermal layer (**Figure 6D & G**). Interestingly, the adipose layer also appeared to be better preserved in MDI-2517 and MMF treated samples, while this layer has almost disappeared in the vehicle controls (compare **Figure 6C to Figure 6D**). MMF-treated animals did not show any improvements in dermal thickness but did show apparent adipose layer preservation (**Figure 6E**). Finally, the combination treatment of MDI-2517 and MMF showed better attenuation of dermal thickening than control or MMF only treated animals (**Figure 6F & G**).

Reduced Lung Fibrosis by MDI-2517 in the Bleomycin Model of SSc

Systemic bleomycin treatment not only causes skin fibrosis but also the subsequent development of lung fibrosis. Therefore, lung histology was examined for fibrosis, and **Figure 7A-F** show closeup images of the fibrotic areas. Similar to the distribution of disease observed in patients with usual interstitial pneumonia, systemic bleomycin exposure induces a pattern of subpleural fibrosis, and this is shown in the low power images in supplemental **Figure S5**. **Figures 7A** and **7B** show lung sections from control mice that received saline pumps and were treated with control chow or chow-containing MDI-2517, respectively. **Figures 7C-F** are representative histopathological sections from mice receiving a bleomycin pump. In contrast to lungs from bleomycin-injured mice treated with control chow, that showed substantial fibrotic changes **(Figure 7C**), lungs from bleomycin-treated mice that received MDI-2517 showed only mild to moderate fibrotic changes (**Figure 7D**). Blinded assessment using the Modified Ashcroft scoring system for lung fibrosis (**Figure 7G**) showed that both MDI-2517 and MMF afforded protection. However, MDI-2517-treated mice showed significantly lower Ashcroft scores than MMF alone (**Figure 7G**). Combination treatment of MDI-2517 and MMF resulted in anti-fibrotic

effects comparable to MDI-2517 treatment alone. Fibrosis was also analyzed in tissue sections stained with picrosirius red to visualize collagen (supplemental **Figure S6**). The images were then quantified based on the intensities of picrosirius red staining (**Figure 7H**) which showed similar results as the Modified Ashcroft scoring system, with MDI-2517, MMF and the combination treatment having significantly reduced collagen compared to the vehicle control.

Comparator Study of MDI-2517 to the PAI-1 inhibitor Tiplaxtinin in the Bleomycin Model of SSc

We next compared the efficacy of MDI-2517 with the PAI-1 inhibitor tiplaxtinin in our bleomycin SSc model. Tiplaxtinin, has been studied in multiple animal models of diverse diseases (29, 30), including in a model of SSc (20). Two different doses of tiplaxtinin were tested: a low dose equivalent to the dose of MDI-2517 (500 mg/kg chow) and a high dose that has been shown to have efficacy in a murine model of atherosclerosis (5 g/kg chow) (31). MDI-2517 showed a significant reduction in skin thickness, while tiplaxtinin at either dose showed no reduction compared to vehicle controls (**Figure 8A**). Additionally, both MDI-2517-treated and animals treated with low-dose tiplaxtinin showed attenuation of weight loss, whereas the high-dose tiplaxtinin-treated cohorts had worse weight loss than control (**Figure 8B**). MDI-2517 treated mice also showed substantially less collagen deposition in the dermal layer (**Figure 9B**) compared to control or either dose of tiplaxtinin. Similar to **Figure 6,** the adipose layer also appeared well preserved in MDI-2517 treated samples, whereas this layer is largely absent in the vehicle controls (**Figure 9A**) as well as in the high-dose tiplaxtinin treated cohort (**Figure 9D**). Quantification of skin thickness based on Mason Trichrome staining (**Figure 9E**) showed similar protection against skin thickening with MDI-2517 treatment as in **Figure 8A**, confirming the efficacy of MDI-2517 in reducing skin thickness using complementary skin pinch and Mason Trichrome staining methods.

Lung histology samples (**Figure 10A-D** and supplementary **Figure S7**) were assessed by Modified Ashcroft scoring for lung fibrosis which demonstrated that both treatment with MDI-

2517 or high-dose tiplaxtinin afforded protection. However, mice treated with MDI-2517 showed significantly lower scores (**Figure 10E**), suggesting MDI-2517 is more efficacious in limiting injury-induced lung fibrosis than tiplaxtinin even at a 10-fold lower dose. This is consistent with previous studies of the closely related PAI-1 inhibitor MDI-2268, which demonstrated an approximate 10-fold higher potency compared to tiplaxtinin both in ex vivo plasma (22) and in vivo (31). MDI-2517 also showed a significant reduction in the amount of picrosirius red staining (approximately 68% less than vehicle control). In contrast, tiplaxtinin showed a non-significant trend toward reduced picrosirius red staining but neither dose attained significance compared to the vehicle control (**Figure 10F** and (supplemental **Figure S8**).

Discussion

SSc is a complex heterogeneous condition characterized by progressive fibrosis in multiple organs. Microvascular dysfunction is thought to be an early event in the development of SSc with vasculopathy and perivascular inflammation promoting fibroblast activation and myofibroblast differentiation (32-34). As vascular injury and perivascular inflammation are among the earliest pathological manifestations observed in SSc, it has been hypothesized that the development of tissue fibrosis in SSc might represent an exaggerated response to vascular damage, ischemia, and inflammation. Therefore, targeting factors with the potential to reduce vascular injury and inflammation has the potential to attenuate fibrotic development and could lead to new therapeutic approaches in SSc.

PAI-1 plays an important role regulating microvascular patency and is best understood for its role in regulating fibrinolysis by inhibiting the tissue-type (tPA) and urokinase-type (uPA) plasminogen activators, which convert the zymogen plasminogen to the active enzyme plasmin (35, 36). It has been shown that in patients with acute and chronic fibrotic diseases, there is a shift away from a net profibrinolytic activity due to a marked induction of PAI-1 (37-42). Recent data from single cell gene expression studies in human lung transplant patients (43) and in the data presented here in SSc skin (**Figures 1 and 2**) demonstrate that PAI-1 expression is prominently increased in these fibrotic disorders. PAI-1 expression is also increased in animal models of pulmonary fibrosis (12, 44-47), and SSc (21). More recently PAI-1 has also been shown to regulate inflammatory cell migration into sites of injury (12, 21, 48, 49). These observations indicate that PAI-1 is a key mediator of pathological vascular and inflammatory responses.

PAI-1 is also a primary regulator of wound healing (50, 51), including in the lung (52), consistent with a critical regulatory role in fibrosis. Wound healing is a natural repair process after injury that consists of overlapping stages, including hemostasis, inflammation, proliferation,

matrix synthesis, and finally, resolution. Disruption of this ordered process can result in impaired wound healing, leading to persistent inflammation and/or matrix synthesis and ultimately to a fibrotic syndrome (53). PAI-1, as a primary regulator of wound healing, has been shown to impact all stages of wound healing, and accordingly, to play a causal role in pulmonary fibrogenesis. Specifically, transgenic mice overproducing PAI-1 have been shown to accumulate excessive collagen following a fibrotic insult (54), whereas mice with a targeted PAI-1 gene deletion have been shown to be resistant to lung fibrosis and have improved survival following lung injury (54, 55). In addition, the suppression of PAI-1 through siRNA or by treatment with a pharmacologic inhibitor limits lung scarring (19, 56). Mechanistically, excess PAI-1 promotes fibrosis by disrupting the ordered process of wound healing at several potential steps. First, by inhibiting fibrinolysis, PAI-1 supports the persistence of the pro-inflammatory provisional hemostatic fibrin matrix (16, 57). Second, PAI-1 enhances inflammatory cell infiltration through direct interaction with cellular integrins (21, 48, 49). This latter process may be particularly relevant to the development of pulmonary fibrosis as PAI-1 has been shown to promote the recruitment of exudate macrophages to the lung (12) and to induce pro-fibrotic M2 polarization in macrophages (58). PAI-1 has also been reported to directly promote myofibroblast differentiation and collagen synthesis (18) and to interact synergistically with TGF-β to sustain the fibrotic response (59-65). Very recently, PAI-1 has also been shown to promote lung fibrosis via a protease independent mechanism through an interaction with sortilin related receptor 1, a mosaic receptor involved in internalizing and intracellular trafficking proteins (14, 66).

Multiple studies have implicated cellular senescence in the pathogenesis of SSc (67, 68), and our previous scRNA-seq analysis of SSc skin found that the highest senescence scores were in fibroblasts, endothelial cells, and pericytes (69). A hallmark of senescent cells is the emergence of the senescence-associated secretory phenotype (SASP) (70). PAI-1 is a well-recognized SASP factor that has been linked to the regulation of cell senescence (65, 71, 72)

and aging (73, 74). The increased expression of PAI-1 in skin fibroblasts reported here is consistent with the high cellular senescence score observed in SSc skin fibroblasts (69), and suggests that, PAI-1 may also exert its pro-fibrotic influence through senescence-related mechanisms. Together these studies indicate that PAI-1 intersects with multiple pathways associated with the development of fibrotic disease and suggest that the inhibition of PAI-1 has the potential to impact the fibrotic response at multiple levels.

The present study demonstrates that the PAI-1 inhibitor MDI-2517 is efficacious in mitigating fibrotic changes in the bleomycin model of SSc. MDI-2517 treatment reduced fibrosis development in the skin in a dose-dependent manner and attenuated weight loss associated with the bleomycin model. Consistent with prior reports that dermal adipocytes play a key role in the pathogenesis of cutaneous fibrosis (75), our histological analyses also revealed that MDI-2517 treatment, in addition to reducing dermal thickening and collagen deposition, also preserved the intradermal adipose layer. Loss of this adipose compartment is a hallmark of fibrotic remodeling, and previous studies have demonstrated that adiponectin-positive adipocyte progenitors can transdifferentiate into myofibroblasts, thereby contributing to fibrosis development (76). Moreover, adipocytes secrete antifibrotic cytokines that may help limit excessive extracellular matrix deposition (77). Thus, the preservation of dermal adipose tissue in MDI-2517-treated animals may underlie, at least in part, the compound's protective effects against bleomycin-induced dermal fibrosis.

Common biomarkers of fibrosis were also reduced by MDI-2517 treatment. Notably, MDI-2517 demonstrates better efficacy than other drugs, such as pirfenidone, MMF, or tiplaxtinin. Further, MDI-2517 demonstrated anti-fibrotic activity in SSc-related lung fibrosis. The first-line standard of care for SSc, MMF, has been shown to slow disease progression; however, it does not stop or reverse progression. Thus, it is imperative that more effective therapeutics be developed. MDI-2517 would be a first-in-class, orally administered once daily, small molecule

inhibitor of PAI-1. Our preclinical data suggests that MDI-2517 may have the potential to halt fibrosis progression, which, if demonstrated in humans, would constitute a substantial advancement over the current standard of care for patients with SSc.

The precise mechanism whereby MDI-2517 reduces fibrogenic progression, collagen accumulation, and disease severity is not known. As discussed above PAI-1 intersects multiple pathways associated with fibrotic disease. Including fibrinolysis, inflammation, senescence, and wound healing, MDI-2517 inhibition of PAI-1 could impact all of these processes. However, the data in **Figure 2** demonstrating the ability of MDI-2517 to significantly down-regulate *COL1A1* and *ACTA2* expression suggests that a major effect of MDI-2517 may be on the myofibroblast phenotype via inhibition of a PAI-1-mediated signaling pathway that promotes fibrogenic gene expression. It is also important to note that, although PAI-1 plays an important role in wound healing, inhibition of PAI-1 with MDI-2517 at the dose used in this study did not appear to impair tissue repair, as no delays in skin wound closure were observed following osmotic pump removal (data not shown). We believe that this is consistent with the reductions in PAI-1 skin and plasma seen in **Figure 3** where MDI-2517 treatment lowers PAI-1 closer to the normal range without producing a state resembling PAI-1 deficiency.

A limitation of our study is that only male mice were used. In humans SSc is more common in women than in men, however men often experience a more severe disease course (78). In our studies we chose to use male mice due to their reported enhanced sensitivity to bleomycin-induced fibrosis compared with females (79, 80). However, in future studies we will compare the response to MDI-2517 treatment in male and female mice to determine if the benefit with seen in male mice is also apparent in females. Another limitation is the lack of pharmacokinetic data due to the administration of drugs via chow, and additional studies with gavage and intravenous dosing will be necessary in the future.

In summary, MDI-2517 has demonstrated remarkable effectiveness in our preclinical model of SSc. However, further studies are warranted to understand the underlying mechanisms by which it exerts its beneficial effects. It will also be important to explore and confirm its efficacy in other preclinical models of fibrosis representative of different organ systems and etiologies. Such studies will provide further understanding of the specific pathways and molecular targets engaged by PAI-1 that are inhibited by MDI-2517 treatment and provide valuable insights into its potential applicability in different organ-specific fibrotic conditions. While the development of targeted therapies for SSc, including those directed at PAI-1, is still in its early stages, these advancements hold promise for the future of SSc treatment. Further research and clinical trials are needed to establish the safety and efficacy of these therapies in future studies.

Materials and Methods

Sex as a biological variable.

The human samples were from both male and female patients and controls (supplemental **Table S2**). Analysis of skin fibroblasts from both male and female donors demonstrated no significant difference in *SERPINE1* expression in either patient or healthy control cells (p=0.668 and p=0.796 respectively). For the mouse experiments, only males were used due to their reported enhanced sensitivity to bleomycin-induced fibrosis compared with females (79, 80), and therefore sex was not considered as a biologic variable.

Patients and Controls.

Study participants were recruited from the University of Michigan Scleroderma Program. Dermal fibroblasts were isolated from punch biopsies from the distal forearm of healthy volunteers and diffuse cutaneous (dc)SSc patients. All patients met the ACR/EULAR criteria for the classification of SSc (81). As summarized in supplemental **Table S2**, all patients were diagnosed with dcSSc (6 males and 20 females; age 54.0 ± 2.7 years, mean ± SEM), and the disease duration was 2.7 ± 0.5 years (mean ± SEM). Their skin scores ranged from 0 to 40 with a mean of 16.3 ± 2.1 (mean ± SEM). Twenty-five patients had Raynaud's phenomenon, 5 had pulmonary arterial hypertension, and 13 had interstitial lung disease at the time of biopsy. Twenty-five patients were on immunosuppressant therapy. Age-, sex-, and ethnicity-matched healthy controls were also recruited (age 52.7 ± 4.4 years, mean ± SEM; 4 males and 12 females). Separately, 22 SSc patients and 18 healthy controls were recruited for single cell RNA-sequencing, and an additional four SSc patients were recruited for spatial-sequencing (23). Skin biopsies were taken from the affected forearms of patients. Both studies were approved by the University of Michigan Institutional Review Board (IRB), and all patients gave written consent. The studies were conducted according to the Declaration of Helsinki Principles.

Single-cell RNA-seq library preparation, sequencing, and alignment

This was performed as previously described by our group (82). After processing Libraries were then sequenced on the Illumina NovaSeq 6000 sequencer to generate 150 bp paired-end reads. Data processing, including quality control, read alignment (hg38), and gene quantification was conducted using the 10X Cell Ranger software. The samples were then merged into a single expression matrix using the cellranger aggr pipeline. The R package Seurat (v3.1.2) was used to cluster the cells in the merged matrix. Cells with less than 500 transcripts or 100 genes or more than 1e5 transcripts or 15% of mitochondrial expression were first filtered out as low-quality cells. Sub-clustering was performed on the abundant cell types. The same functions described above were used to obtain the sub-clusters. Sub-clusters that were defined exclusively by mitochondrial gene expression, indicating low quality, were removed from further analysis.

Spatial sequencing library preparation

Skin samples were frozen in OCT medium and stored at -80°C until sectioning. Optimization of tissue permeabilization was performed on 20 μm sections using Visium Spatial Tissue Optimization Reagents Kit (10X Genomics, Pleasanton, CA, USA), which established an optimal permeabilization time to be 9 minutes. Samples were mounted onto a Gene Expression slide (10X Genomics). Libraries were then sequenced on the Illumina NovaSeq 6000 sequencer to generate 150 bp paired end reads. After sequencing, the reads were aligned to the human genome (hg38), and the expression matrix was extracted using the spaceranger pipeline. Seurat was then used to analyze the expression matrix. Specifically, the SCTransform function was used to scale the data and find variable genes with default parameters. PCA and UMAP were applied for dimensional reduction. The FindTransferAnchors function was used to find a set of anchors between the spatial-seq data and scRNA-seq data, which were then transferred from the scRNA-seq to the spatial-seq data using the TransferData function

Immunohistochemistry staining

Paraffin embedded tissue sections from human skin (SSc and normal) were heated at 60°C for 30 minutes, de-paraffinized, rehydrated, and counter stained with hematoxylin. Slides were placed in PH9 antigen retrieval buffer and heated at 125°C for 30 seconds in a pressure cooker. After cooling, slides were treated with 3% H_2O_2 for 5 minutes and then blocked using 10% goat serum for 30 minutes. Overnight incubation (4°C) was then performed using anti-human PAI-1 (Innovative Research, ASHPAI-GF-HT) at a dilution of 1:300. Slides were then washed, treated with peroxidase labeled secondary antibody (Abcam, ab6802), for 30 minutes and reacted with the diaminobenzidine substrate.

Cell culture

Punch biopsies obtained from healthy subjects and SSc patients were digested as previously described (83, 84). Dermal fibroblasts were maintained in RPMI supplemented with 10% fetal bovine serum (FBS), L-glutamine, and antibiotics. Cells between passage 3 and 6 were used in all experiments.

Cell treatment

Dermal fibroblasts from dcSSc patients were treated with 100 μM of MDI-2517 or vehicle for 48 hours prior to qRT-PCR measurement for *ACTA2* and *COL1A1* and for 72 hours prior to immunoblotting of αSMA and COL1 .

mRNA extraction and qRT-PCR

Total RNA was extracted using Direct-zol™ RNA MiniPrep Kit (Zymo Research) before being converted to cDNA using the Verso cDNA synthesis kit (Thermo Fisher). Quantitative PCR was performed using SYBR Green PCR Master Mix (Applied Biosystems) with specific primers for *COL1A1, ACTA2, SERPINE1*, with *ACTB* as reference gene for normalization. We assessed *ACTB* expression levels across the SSc fibroblast and healthy controls and found no significant differences confirming its suitability as a reference gene (KiCqStart® SYBR® Green Primers,

Millipore Sigma). All samples were run in duplicate using the ViiA™ 7 Real-Time PCR System. Data was analyzed using the Applied Biosystems software.

Western blots

Western blotting was performed following the protocol as described previously (84). Briefly, equal amounts of cell lysates were loaded onto polyacrylamide gels and separated by SDS-PAGE. The proteins were then transferred onto nitrocellulose membranes via Western blotting. After blocking, the blots were probed with antibodies against collagen I (Abcam ab6308), PAI-1 (Innovative Research, IRBAHUPAI1AP100UG), or αSMA (Abcam ab5694). For loading control, the blots were immunoblotted with antibodies against GAPDH (Cell Signaling #2118) or vinculin (Sigma Aldrich, V9131). Band quantification was performed using ImageJ (85) or with Image Studio (Licorbio).

Murine model of SSc

All animal procedures were performed in accordance with the local welfare legislation and approved by the Institutional Animal Care and Use Committees at the University of Michigan. Twelve-week-old male C57BL/6 mice (Jackson Lab) received bleomycin via osmotic minipumps (ALZET 1007D, DURECT, Cupertino, CA). The minipumps were loaded with bleomycin (100 U/kg). Mice were anesthetized with isofluorane and the pumps were implanted subcutaneously under the loose skin on the back of the mice slightly posterior to the scapulae. Pumps were removed on day 7 as recommended by the manufacturer. The incision was closed with a wound clip. After pump removal, animals were placed on synthetic laboratory chow (Dyets Inc, Bethlehem, Pennsylvania) supplemented with PAI-1 inhibitor, MDI-2517 (MDI Therapeutics Inc., Novi MI) at various doses (250 mg/kg, 500 mg/kg and 1000 mg/kg), pirfenidone (Cipla, Mumbai India) (1000 mg/kg), mycophenolate (Accord Health, Devon, England) (1000 mg/kg), tiplaxtinin (synthesized by Dr. Scott D. Larsen University of Michigan College of Pharmacy as described (86) high dose (5000 mg/kg), tiplaxtinin low dose (500 mg/kg) or control chow without any

drugs. The amount chow consumed for each formulation was monitored by cages to ensure that there were no significant differences between groups. For all studies presented except the pilot study in figure S3, all mice receiving bleomycin were given daily subcutaneous saline injections (10mL/kg) from Day 9 to day 16 to prevent dehydration. This reduced overall mortality from 20% (4 of 20) in the pilot study to 2.7% (3 of 110) in all other studies. Control groups not treated with bleomycin were not give saline injections.

Tissue collection

Four weeks after pump implantation, mice were anesthetized and transcardially perfused with PBS and then the trachea was cannulated, and the lung tissues were inflated and fixed with 10% neutral phosphate-buffered formalin *in situ*. The fixed lungs were processed and embedded in paraffin for microscopy. Skin samples were collected at the region of pump delivery as well as an area approximately 5 cm away and processed for histology.

Morphometric Analysis

For histopathological evaluation of fibrosis, mouse lungs, and skin were fixed in 10% neutral phosphate-buffered formalin. The paraffin-embedded tissues were cut into 5-μm sections and stained with Masson's trichrome. Fibrosis was assessed using a modified Ashcroft score for lung tissues, with a numerical fibrosis scoring scale (0-8), in Masson's trichrome-stained sections (87). Scoring was performed by a blinded investigator. Dermal thickness was measured in Masson's trichrome-stained sections by measuring the distance between the epidermal–dermal junction and the dermal–fat junction in five randomly selected fields in two or more sections from each animal. The data shown are from the skin samples collected proximal to pump delivery.

Picrosirius Red Staining and Quantification

Deparaffinization sections (5 μm) were immersed in picrosirius red solution (0.1% w/v Direct Red 80 (Sigma 365548; St. Louis, MO) in a saturated aqueous solution of picric acid (Sigma) for 1 hour. Sections were briefly rinsed in two changes of acidified dH20 (0.5% glacial acetic acid), dehydrated, cleared, and mounted. Digital images obtained with a Nikon Microphot-SA microscope and Nikon DS-Fi3 camera (Nikon Inc., Melville, NY) were obtained by NIS Elements software and analyzed using Image J software. Microscope conditions (lamp brightness, condenser opening, objective, zoom, exposure time, and gain parameters) were maintained throughout the imaging of all samples. Collagen content was quantified using signal threshold settings.

PAI-1 and Biomarkers quantification

Selected biomarkers including surfactant proteins (SP-D), intercellular adhesion molecule 1 (ICAM-1), and Matrix Metallopeptidase 9 (MMP 9) were quantified in plasma samples from mice drawn on day 28 at the time the mice were sacrificed, and biomarkers measured on a Luminex X-100 (Luminex Corporation, Austin, TX) using a 3-plex Luminex panel (LXSAMSM-03, R&D Systems). The concentration of total and active murine PAI-1 in plasma was measured using a magnetic carboxylated microsphere-based ELISA as previously described (14).

Immunofluorescence

Quantification of PAI-1 immunofluorescence in mouse skin tissue was obtained from 5μm-thick paraffin sections. Slides were dried on slide warmer at 55 degrees C. Slides were deparaffinized with Histoclear and rehydrated by incubating through a graded series of ethanol from 100% to 50% and rinsed with tap water. Slides are then rinsed in PBS, and subjected to antigen retrieval (S1700, Dako), then permeabilized in PBS+0.5% TritonX-100 (PBST) after which they were blocked overnight with PBST+ 5% Bovine Serum Albumin. Sections were next incubated with primary antibody (monoclonal H34G6, Innovative Research. Novi, Mi) in PBST with 1% horse serum for 2 hours at RT, washed 3X with PBST and then developed with a secondary antibody-

568 Alexa-Fluor incubation of 1 hour RT. Sections are washed 3x with PBST and incubated in PBST + Dapi for a final 10-minute incubation at RT. Sections are washed 3x with PBST and a final wash in PBS alone. Coverslips are added to slides with Vectorshield hardset mounting media (H1400-10, Vector Laboratories). Digital images were captured by a Nikon Microphot-SA microscope and PCO Panda camera (Nikon Inc., Melville, NY) with NIS Elements software and analyzed using Image J software. PAI-1 levels were quantified using signal threshold settings.

Statistics

Data analysis was performed using GraphPad Prism 8 statistical software (GraphPad Software, La Jolla, CA, USA). For in vivo experiments n indicates the number of individual mice used in the study. For statistical analysis, in any experiment with only two groups, a two-tailed t-test or Mann-Whitney test was used. For experiments with more than two groups, a one-way ANOVA with appropriate post hoc test for multiple comparisons except for qPCR comparisons where a one sample Wilcoxon test was used. For analysis of weight loss, the data were analyzed by a repeated measures mixed-effect model with an appropriate post hoc test for multiple comparisons. In all graphs the relevant statistical comparisons are shown, and all statistical comparisons are given in supplementary **Table S3**. Data is represented as mean values ± SD; $p < 0.05$ was considered significant.

Study approval

The study was approved by the University of Michigan Institutional Review Board (IRB), and all patients gave written consent. The study was conducted according to the Declaration of Helsinki Principles. All animals were housed in the University of Michigan animal facility, provided food and water ad libitum, and all procedures were conducted under approved University of Michigan Institutional Animal Care and Use protocols.

Data availability

The RNAseq data can be accessed on GEO GSE249279. All data from this study are accessible in Supplemental Data, Supporting Data Values file, and public repositories.

Author contributions

EJS, and PST designed and performed experiments, analyzed data, and wrote the manuscript, MW, NS. KM, SV, AR, LL, XX, EX, OP, RB, and LCT performed experiments and acquired data; CDE provided reagents and edited the manuscript; DK, JV, and THS, provided advice on experiments and edited the manuscript JEG and DAL designed experiments, analyzed data, and wrote the manuscript. All authors read and approved the final manuscript.

Acknowledgments

This research was supported by Grants to D.A.L. from the National Heart, Lung, and Blood Institute of the National Institutes of Health Awards R01HL055374 and R01HL163870, the National Institute On Aging of the National Institutes of Health Award Number R01AG074552, and by subcontracts to DAL from MDI Therapeutics from the National Institute Of Arthritis and Musculoskeletal and Skin Diseases of the National Institutes of Health awards R43AR074318 and R44AR074318, and the National Heart, Lung, and Blood Institute of the National Institutes of Health awards R43HL145960 and R44HL158435.

References

1. Denton CP, and Khanna D. Systemic sclerosis. *Lancet.* 2017;390(10103):1685-99.
2. Allanore Y, et al. Systemic sclerosis. *Nat Rev Dis Primers.* 2015;1:15002.
3. Tyndall AJ, et al. Causes and risk factors for death in systemic sclerosis: a study from the EULAR Scleroderma Trials and Research (EUSTAR) database. *Ann Rheum Dis.* 2010;69(10):1809-15.
4. Hax V, et al. Clinical algorithms for the diagnosis and prognosis of interstitial lung disease in systemic sclerosis. *Semin Arthritis Rheum.* 2017;47(2):228-34.
5. Bergamasco A, et al. Epidemiology of systemic sclerosis and systemic sclerosis-associated interstitial lung disease. *Clin Epidemiol.* 2019;11:257-73.
6. Volkmann ER, and Fischer A. Update on Morbidity and Mortality in Systemic Sclerosis-Related Interstitial Lung Disease. *J Scleroderma Relat Disord.* 2021;6(1):11-20.
7. Nakayama Y, et al. Prognosis of patients with systemic sclerosis-related interstitial lung disease on the lung transplant waiting list: a retrospective study. *Sci Rep.* 2023;13(1):10150.
8. Gabrielli A, Avvedimento EV, and Krieg T. Scleroderma. *N Engl J Med.* 2009;360(19):1989-2003.
9. Denton CP. Systemic sclerosis: from pathogenesis to targeted therapy. *Clin Exp Rheumatol.* 2015;33(4 Suppl 92):S3-S7.
10. Ferrari HM, et al. Systemic-Sclerosis-Related Interstitial Lung Disease: A Review of the Literature and Recommended Approach for Clinical Pharmacists. *Ann Pharmacother.* 2023:10600280231213672.
11. Lemaire R, et al. Resolution of Skin Fibrosis by Neutralization of the Antifibrinolytic Function of Plasminogen Activator Inhibitor 1. *Arthritis Rheumatol.* 2016;68(2):473-83.
12. Osterholzer JJ, et al. PAI-1 promotes the accumulation of exudate macrophages and worsens pulmonary fibrosis following type II alveolar epithelial cell injury. *J Pathol.* 2012;228(2):170-80.
13. Zhong J, et al. Vitronectin-binding PAI-1 protects against the development of cardiac fibrosis through interaction with fibroblasts. *Lab Invest.* 2014;94(6):633-44.
14. Courey AJ, et al. The vitronectin-binding function of PAI-1 exacerbates lung fibrosis in mice. *Blood.* 2011;118(8):2313-21.
15. Kanno Y. The Role of Fibrinolytic Regulators in Vascular Dysfunction of Systemic Sclerosis. *Int J Mol Sci.* 2019;20(3).
16. Ghosh AK, and Vaughan DE. PAI-1 in tissue fibrosis. *J Cell Physiol.* 2012;227(2):493-507.
17. Stifano G, et al. Skin Gene Expression Is Prognostic for the Trajectory of Skin Disease in Patients With Diffuse Cutaneous Systemic Sclerosis. *Arthritis Rheumatol.* 2018;70(6):912-9.
18. Omori K, et al. Inhibition of Plasminogen Activator Inhibitor-1 Attenuates Transforming Growth Factor-beta-Dependent Epithelial Mesenchymal Transition and Differentiation of Fibroblasts to Myofibroblasts. *PLoS One.* 2016;11(2):e0148969.
19. Huang WT, et al. Therapeutic value of small molecule inhibitor to plasminogen activator inhibitor-1 for lung fibrosis. *Am J Respir Cell Mol Biol.* 2012;46(1):87-95.
20. Zou ML, et al. The uPA System Differentially Alters Fibroblast Fate and Profibrotic Ability in Skin Fibrosis. *Front Immunol.* 2022;13:845956.
21. Pincha N, et al. PAI1 mediates fibroblast-mast cell interactions in skin fibrosis. *J Clin Invest.* 2018;128(5):1807-19.
22. Reinke AA, et al. Dual-reporter high-throughput screen for small-molecule in vivo inhibitors of plasminogen activator inhibitor type-1 yields a clinical lead candidate. *J Biol Chem.* 2019;294(5):1464-77.
23. Ma F, et al. Systems-based identification of the Hippo pathway for promoting fibrotic mesenchymal differentiation in systemic sclerosis. *Nat Commun.* 2024;15(1):210.

24. Ravanetti F, et al. SSC-ILD mouse model induced by osmotic minipump delivered bleomycin: effect of Nintedanib. *Sci Rep.* 2021;11(1):18513.
25. Huerkamp MJ, and Dowdy MR. Diet replenishment for ad-libitum-fed mice housed in social groups is compatible with shelf life. *J Am Assoc Lab Anim Sci.* 2008;47(3):47-50.
26. Cale JM, et al. Characterization of a novel class of polyphenolic inhibitors of plasminogen activator inhibitor-1. *J Biol Chem.* 2010;285(11):7892-902.
27. Tashkin DP, et al. Cyclophosphamide versus placebo in scleroderma lung disease. *N Engl J Med.* 2006;354(25):2655-66.
28. Acharya N, et al. Efficacy and safety of pirfenidone in systemic sclerosis-related interstitial lung disease-a randomised controlled trial. *Rheumatol Int.* 2020;40(5):703-10.
29. Gorlatova NV, et al. Mechanism of inactivation of plasminogen activator inhibitor-1 by a small molecule inhibitor. *J Biol Chem.* 2007;282(12):9288-96.
30. Baxi S, et al. Dose-dependent thrombus resolution due to oral plaminogen activator inhibitor (PAI)-1 inhibition with tiplaxtinin in a rat stenosis model of venous thrombosis. *Thromb Haemost.* 2008;99(4):749-58.
31. Khoukaz HB, et al. Drug Targeting of Plasminogen Activator Inhibitor-1 Inhibits Metabolic Dysfunction and Atherosclerosis in a Murine Model of Metabolic Syndrome. *Arterioscler Thromb Vasc Biol.* 2020:ATVBAHA119313775.
32. Zanin-Silva DC, et al. Management of Endothelial Dysfunction in Systemic Sclerosis: Current and Developing Strategies. *Front Med (Lausanne).* 2021;8:788250.
33. Leask A, Naik A, and Stratton RJ. Back to the future: targeting the extracellular matrix to treat systemic sclerosis. *Nat Rev Rheumatol.* 2023.
34. Lescoat A, Lecureur V, and Varga J. Contribution of monocytes and macrophages to the pathogenesis of systemic sclerosis: recent insights and therapeutic implications. *Curr Opin Rheumatol.* 2021;33(6):463-70.
35. Cesari M, Pahor M, and Incalzi RA. Plasminogen activator inhibitor-1 (PAI-1): a key factor linking fibrinolysis and age-related subclinical and clinical conditions. *Cardiovasc Ther.* 2010;28(5):e72-91.
36. Humphreys SJ, Whyte CS, and Mutch NJ. "Super" SERPINs-A stabilizing force against fibrinolysis in thromboinflammatory conditions. *Front Cardiovasc Med.* 2023;10:1146833.
37. Simon R, Edwards J, and RG S. Fibrin is rapidly formed and lysed when plasma is introduced into the alveolar space of intact lungs. *Am J Respir Crit Care Med.* 1995;151:A344.
38. Chapman HA, Allen CL, and Stone OL. Abnormalities in pathways of alveolar fibrin turnover among patients with interstitial lung disease. *Am Rev Respir Dis.* 1986;133(3):437-43.
39. Bertozzi P, et al. Depressed bronchoalveolar urokinase activity in patients with adult respiratory distress syndrome. *N Engl J Med.* 1990;322(13):890-7.
40. Viscardi RM, et al. Disordered pathways of fibrin turnover in lung lavage of premature infants with respiratory distress syndrome. *Am Rev Respir Dis.* 1992;146(2):492-9.
41. Kotani I, et al. Increased procoagulant and antifibrinolytic activities in the lungs with idiopathic pulmonary fibrosis. *Thromb Res.* 1995;77(6):493-504.
42. Prabhakaran P, et al. Elevated levels of plasminogen activator inhibitor-1 in pulmonary edema fluid are associated with mortality in acute lung injury. *Am J Physiol Lung Cell Mol Physiol.* 2003;285(1):L20-L8.
43. Reyfman PA, et al. Single-Cell Transcriptomic Analysis of Human Lung Provides Insights into the Pathobiology of Pulmonary Fibrosis. *Am J Respir Crit Care Med.* 2019;199(12):1517-36.
44. Idell S, et al. Abnormalities of pathways of fibrin turnover in lung lavage of rats with oleic acid and bleomycin-induced lung injury support alveolar fibrin deposition. *Am J Pathol.* 1989;135(2):387-99.

45. Idell S, et al. Local abnormalities of coagulation and fibrinolytic pathways that promote alveolar fibrin deposition in the lungs of baboons with diffuse alveolar damage. *J Clin Invest.* 1989;84(1):181-93.
46. Idell S, James KK, and Coalson JJ. Fibrinolytic activity in bronchoalveolar lavage of baboons with diffuse alveolar damage: trends in two forms of lung injury. *Crit Care Med.* 1992;20(10):1431-40.
47. Olman MA, et al. Changes in procoagulant and fibrinolytic gene expression during bleomycin-induced lung injury in the mouse. *J Clin Invest.* 1995;96(3):1621-30.
48. Cao C, et al. Endocytic receptor LRP together with tPA and PAI-1 coordinates Mac-1-dependent macrophage migration. *EMBO J.* 2006;25(9):1860-70.
49. Praetner M, et al. Plasminogen Activator Inhibitor-1 Promotes Neutrophil Infiltration and Tissue Injury on Ischemia-Reperfusion. *Arterioscler Thromb Vasc Biol.* 2018;38(4):829-42.
50. Chan JC, et al. Accelerated skin wound healing in plasminogen activator inhibitor-1-deficient mice. *Am J Pathol.* 2001;159(5):1681-8.
51. Simone TM, et al. Targeted Inhibition of PAI-1 Activity Impairs Epithelial Migration and Wound Closure Following Cutaneous Injury. *Adv Wound Care (New Rochelle).* 2015;4(6):321-8.
52. Lazar MH, et al. Plasminogen activator inhibitor-1 impairs alveolar epithelial repair by binding to vitronectin. *Am J Respir Cell Mol Biol.* 2004;31(6):672-8.
53. Diegelmann RF, and Evans MC. Wound healing: an overview of acute, fibrotic and delayed healing. *Front Biosci.* 2004;9:283-9.
54. Eitzman DT, et al. Bleomycin-induced pulmonary fibrosis in transgenic mice that either lack or overexpress the murine plasminogen activator inhibitor-1 gene. *J Clin Invest.* 1996;97(1):232-7.
55. Hattori N, et al. Bleomycin-induced pulmonary fibrosis in fibrinogen-null mice. *J Clin Invest.* 2000;106(11):1341-50.
56. Senoo T, et al. Suppression of plasminogen activator inhibitor-1 by RNA interference attenuates pulmonary fibrosis. *Thorax.* 2010;65(4):334-40.
57. Tucker T, and Idell S. Plasminogen-plasmin system in the pathogenesis and treatment of lung and pleural injury. *Semin Thromb Hemost.* 2013;39(4):373-81.
58. Kubala MH, et al. Plasminogen Activator Inhibitor-1 Promotes the Recruitment and Polarization of Macrophages in Cancer. *Cell Rep.* 2018;25(8):2177-91 e7.
59. Abe M, et al. An assay for transforming growth factor-beta using cells transfected with a plasminogen activator inhibitor-1 promoter-luciferase construct. *Anal Biochem.* 1994;216(2):276-84.
60. Lund LR, et al. Transforming growth factor-beta is a strong and fast acting positive regulator of the level of type-1 plasminogen activator inhibitor mRNA in WI-38 human lung fibroblasts. *EMBO J.* 1987;6(5):1281-6.
61. Dennler S, et al. Direct binding of Smad3 and Smad4 to critical TGF beta-inducible elements in the promoter of human plasminogen activator inhibitor-type 1 gene. *EMBO J.* 1998;17(11):3091-100.
62. Samarakoon R, Overstreet JM, and Higgins PJ. TGF-beta signaling in tissue fibrosis: redox controls, target genes and therapeutic opportunities. *Cell Signal.* 2013;25(1):264-8.
63. Rabieian R, et al. Plasminogen Activator Inhibitor Type-1 as a Regulator of Fibrosis. *J Cell Biochem.* 2018;119(1):17-27.
64. Hu PF, et al. Inhibition of plasminogen activator inhibitor-1 expression by siRNA in rat hepatic stellate cells. *J Gastroenterol Hepatol.* 2008;23(12):1917-25.
65. Rana T, et al. PAI-1 Regulation of TGF-beta1-induced Alveolar Type II Cell Senescence, SASP Secretion, and SASP-mediated Activation of Alveolar Macrophages. *Am J Respir Cell Mol Biol.* 2020;62(3):319-30.

66. Sisson TH, et al. PAI-1 interaction with sortilin-related receptor 1 is required for lung fibrosis. *JCI Insight.* 2025;10(11).
67. Tsou PS, Shi B, and Varga J. Role of cellular senescence in the pathogenesis of systemic sclerosis. *Curr Opin Rheumatol.* 2022;34(6):343-50.
68. Yang MM, Boin F, and Wolters PJ. Molecular underpinnings of aging contributing to systemic sclerosis pathogenesis. *Curr Opin Rheumatol.* 2025;37(1):86-92.
69. Shi B, et al. Senescent Cells Accumulate in Systemic Sclerosis Skin. *J Invest Dermatol.* 2023;143(4):661-4 e5.
70. Basisty N, et al. A proteomic atlas of senescence-associated secretomes for aging biomarker development. *PLoS Biol.* 2020;18(1):e3000599.
71. Ozcan S, et al. Unbiased analysis of senescence associated secretory phenotype (SASP) to identify common components following different genotoxic stresses. *Aging (Albany NY).* 2016;8(7):1316-29.
72. Vaughan DE, et al. Plasminogen Activator Inhibitor-1 Is a Marker and a Mediator of Senescence. *Arterioscler Thromb Vasc Biol.* 2017;37(8):1446-52.
73. Eren M, et al. PAI-1-regulated extracellular proteolysis governs senescence and survival in Klotho mice. *Proc Natl Acad Sci U S A.* 2014;111(19):7090-5.
74. Khan SS, et al. A null mutation in SERPINE1 protects against biological aging in humans. *Sci Adv.* 2017;3(11):eaao1617.
75. Varga J, and Marangoni RG. Systemic sclerosis in 2016: Dermal white adipose tissue implicated in SSc pathogenesis. *Nat Rev Rheumatol.* 2017;13(2):71-2.
76. Marangoni RG, et al. Myofibroblasts in murine cutaneous fibrosis originate from adiponectin-positive intradermal progenitors. *Arthritis Rheumatol.* 2015;67(4):1062-73.
77. Peng Y, et al. Dermal white adipose tissue: Development and impact on hair follicles, skin defense, and fibrosis. *FASEB J.* 2024;38(18):e70047.
78. Toitou M, et al. Sex differences in systemic sclerosis: from pathogenesis to clinical manifestations and treatment. *Ther Adv Musculoskelet Dis.* 2025;17:1759720X251384602.
79. Voltz JW, et al. Male sex hormones exacerbate lung function impairment after bleomycin-induced pulmonary fibrosis. *Am J Respir Cell Mol Biol.* 2008;39(1):45-52.
80. Redente EF, et al. Age and sex dimorphisms contribute to the severity of bleomycin-induced lung injury and fibrosis. *Am J Physiol Lung Cell Mol Physiol.* 2011;301(4):L510-8.
81. van den Hoogen F, et al. 2013 classification criteria for systemic sclerosis: an American college of rheumatology/European league against rheumatism collaborative initiative. *Ann Rheum Dis.* 2013;72(11):1747-55.
82. Ma F, et al. Single cell and spatial sequencing define processes by which keratinocytes and fibroblasts amplify inflammatory responses in psoriasis. *Nat Commun.* 2023;14(1):3455.
83. Tsou PS, et al. Inhibition of EZH2 prevents fibrosis and restores normal angiogenesis in scleroderma. *Proc Natl Acad Sci U S A.* 2019;116(9):3695-702.
84. Tsou PS, Khanna D, and Sawalha AH. Identification of Cysteine-Rich Angiogenic Inducer 61 as a Potential Antifibrotic and Proangiogenic Mediator in Scleroderma. *Arthritis Rheumatol.* 2019;71(8):1350-9.
85. Schneider CA, Rasband WS, and Eliceiri KW. NIH Image to ImageJ: 25 years of image analysis. *Nature Methods.* 2012;9:671.
86. Elokdah H, et al. Tiplaxtinin, a novel, orally efficacious inhibitor of plasminogen activator inhibitor-1: design, synthesis, and preclinical characterization. *J Med Chem.* 2004;47(14):3491-4.
87. Hubner RH, et al. Standardized quantification of pulmonary fibrosis in histological samples. *Biotechniques.* 2008;44(4):507-11, 14-7.

Figure Legends

Figure 1. Expression of PAI-1 in SSc skin. A) Comparison of *SERPINE1* expression in SSc and healthy control skin biopsy samples from the GEO dataset (GSE58095). B) Correlation analysis of mRSS scores vs. *SERPINE1* expression from the data in A. C) Enriched signature for expression of extracellular matrix (ECM) genes along with expression of the myofibroblasts marker *COL8A1*, and *SERPINE1* (PAI-1) expression in SSc skin on the 10X Visium spatial platform (data representative of n=4). D) Violin plots of *SERPINE1* expression in controls vs. SSc skin across scRNA-seq data from different cellular populations (upper panel) and fibroblast subsets (lower panel). (n=18 healthy controls, n=22 SSc patients) E) Enriched biological processes in *SERPINE1*+ vs. *SERPINE1*- *COL8A1* myofibroblasts. F) IHC of PAI-1 in SSc skin biopsy (data representative of n=6). G) IHC of PAI-1 in skin biopsy from a healthy volunteer. Scale bar on overall biopsy is 500um, and 50um on the inserts. **** $p<0.0001$, by two tail Mann-Whitney test in panel A and $p=0.0003$ by Spearmann r correlation test in panel B.

Figure 2. Downregulate pro-fibrotic markers in human SSc fibroblasts by MDI-2517. Dermal fibroblasts were isolated from punch biopsies from the distal forearm of healthy volunteers and diffuse cutaneous (dc)SSc patients. A) QPCR of PAI-1 (*SERPINE1*) mRNA expression in fibroblasts from normal skin and from SSc patients. B) Downregulate mRNA expression of pro-fibrotic markers, SMA and *COL1A1*, with MDI-2517 treatment. C) Western blot analysis shows reduction in COL1, SMA, and PAI-1 protein in SSc fibroblasts with and without MDI-2517 treatment. D) Quantification of the western blots in C, SMA and *COL1A1* are shown as the ratio to GAPDH and PAI-1 to vinculin. Data is shown as mean ± SD, n is indicated in each figure by the individual data points (3-17), * $p<0.05$, ** $p<0.01$, *** $p<0.001$, by two-tailed Mann-Whitney test in A, by a one sample Wilcoxon in B, and a two-tailed t test in D.

Figure 3. Target engagement of MDI-2517. Twelve-week-old male C57BL/6J mice were subcutaneously implanted with osmotic pumps that deliver 100U/kg (total) of bleomycin over 7 days. The pumps were then removed, and at that time the mice were placed on chow containing 0 mg/kg (Vehicle) or MDI-2517 at 500 mg/kg chow. On day 28 skin tissue and plasma and were collected. PAI-1 antigen in skin was quantified by immunofluorescence microscopy, images were acquired using the same settings and taken in comparable regions for each skin sample. For quantification 5 areas of interest per skin sample were analyzed (n=4 mice per treatment group) and the area of antibody immunoreactivity above a set threshold was measured and averaged for each animal using ImageJ. Panel A) Immunofluorescent staining of PAI-1 (red) and DAPI nuclear stain (blue), hematoxylin and eosin (H&E) and Picrosirius Red staining. Panel B) Quantification of the relative PAI-1 antigen in skin of the untreated and MDI-2517 treated mice. Panel C) Active and total PAI-1 in plasma. Data is shown as mean ± SD, n is indicated in each figure by the individual data points (4-5), scale bar = 100μm, * $p<0.05$ in panel B, ** $p<0.01$ in panel C, by two-tailed t-test.

Figure 4. Comparator study of MDI-2517, pirfenidone and mycophenolate mofetil (MMF). Twelve-week-old male C57BL/6J mice were subcutaneously implanted with osmotic pumps that deliver 100U/kg (total) of bleomycin over 7 days. The pumps were then removed, and at that time the mice were placed on treatment chows (drug concentration in chow: Vehicle, 0mg/kg, MDI-2517 at 500mg/kg, pirfenidone at 1000mg/kg, MMF at 1000mg/kg). A) On day 28 skin thickness is determined at multiple locations by skin pinch with calipers then sacrificed and plasma and skin tissues collected. B) Body weight changes monitored approximately every 3 days. C-E) Biomarkers measured by antibody based Luminex multiplex assay. Data is shown as mean ± SD, n is indicated in each figure by the individual data points (4-5), * $p<0.05$, ** $p<0.01$, *** $p<0.001$, **** $p<0.0001$, by one-way ANOVA in panels A, C-E and by a repeated measures mixed-effect model in panel B.

Figure 5, Comparator study of MDI-2517, mycophenolate (MMF) and MMF+MDI-2517. Twelve-week-old male C57BL/6J mice were subcutaneously implanted with osmotic pumps that deliver 100U/kg (total) of bleomycin over 7 days. The pumps were then removed, and at that time the mice were placed on treatment chows (drug concentration in chow: Vehicle, 0 mg/kg, MDI-2517 at 500 mg/kg, MMF at 1000mg/kg or combined MDI-2517 at 500 mg/kg and MMF at 1000 mg/kg,). A) On day 28 skin thickness was determined at multiple locations by skin pinch with calipers then sacrificed and tissues collected. B) Body weight changes monitored approximately every 3 days. Data is shown as mean ± SD, n is indicated in each figure by the individual data points (5-8), * $p<0.05$, ** $p<0.01$, **** $p<0.0001$, by one-way ANOVA in panel A and by a repeated measures mixed-effect model in panel B.

Figure 6, Skin trichrome staining from the comparator study of MDI-2517, mycophenolate (MMF) and combined MMF+MDI-2517. Twelve-week-old male C57BL/6J mice were subcutaneously implanted with osmotic pumps that deliver 100U/kg (total) of bleomycin or saline over 7 days. The pumps were then removed, and at that time the mice were placed on treatment chows (drug concentration in chow: Vehicle, 0 mg/kg, MDI-2517 at 500 mg/kg, MMF at 1000mg/kg or combined MDI-2517 at 500 mg/kg and MMF at 1000 mg/kg,). On day 28, skin tissues were prepared for histological analysis by Mason Trichrome Stain. A) Saline pump Control Chow, B) Saline pump MDI-2517 chow, C) Bleomycin control chow (No Treatment), D) Bleomycin MDI-2517 chow, E) Bleomycin MMF chow, F) Bleomycin combined MMF and MDI-2517 chow, G) Quantification of skin thickness from Mason Trichrome stained slides. Data is shown as mean ± SD, n is indicated in each figure by the individual data points (5-8), scale bar = 100μm, ** $p<0.01$, *** $p<0.001$, **** $p<0.0001$, by one-way ANOVA.

Figure 7, Lung trichrome staining from the comparator study of MDI-2517, mycophenolate (MMF) and combined MMF+MDI-2517. Twelve-week-old male C57BL/6J mice were implanted with osmotic pumps that deliver 100U/kg (total) of bleomycin or saline over 7 days. The pumps were then removed, and at that time the mice were placed on treatment chows (drug concentration in chow: Vehicle, 0 mg/kg, MDI-2517 at 500 mg/kg, MMF at 1000mg/kg or combined MDI-2517 at 500 mg/kg and MMF at 1000 mg/kg,). On day 28, lung tissues were prepared for histological analysis by Mason Trichrome stain and Picrosirius Red stain. A) Saline pump Control Chow, B) Saline pump MDI-2517 chow, C) Bleomycin control chow (No Treatment), D) Bleomycin MDI-2517 chow, E) Bleomycin MMF chow, F) Bleomycin combined MMF and MDI-2517 chow, G) Ashcroft Modified score of lung tissue from Mason Trichrome stained slides, H) Picrosirius Red quantification from stained slides. Data is shown as mean ± SD, n is indicated in each figure by the individual data points (5-8), scale bar = 35μm, * $p<0.05$, **** $p<0.0001$, by one-way ANOVA in panel G and H.

Figure 8, Comparator Study MDI-2517, Tiplaxtinin Low and High Dose. Twelve-week-old male C57BL/6J mice were subcutaneously implanted with osmotic pumps that deliver 100U/kg (total) of bleomycin over 7 days. The pumps were then removed, and at that time the mice were placed on treatment chows (drug concentration in chow: Vehicle, 0 mg/kg, MDI-2517 at 500 mg/kg, tiplaxtinin Low dose at 500 mg/kg or tiplaxtinin High dose at 5000 mg/kg). A) On day 28 skin thickness is determined at multiple locations by skin pinch with calipers then sacrificed and tissues collected. B) Body weight changes monitored approximately every 3 days. Data is shown as mean ± SD, n is indicated in each figure by the individual data points (10), ** $p<0.01$,*** $p<0.001$, **** $p<0.0001$, by one-way ANOVA in panel A and by a repeated measures mixed-effect model in panel B.

Figure 9, Skin thickness by Mason Trichrome from comparator Study MDI-2517, Tiplaxtinin Low and High Dose. Twelve-week-old male C57BL/6J mice were subcutaneously implanted with osmotic pumps that deliver 100U/kg (total) of bleomycin over 7 days. The pumps were then removed, and at that time the mice were placed on treatment chows (drug concentration in chow: Vehicle, 0 mg/kg, MDI-2517 at 500 mg/kg, tiplaxtinin Low dose at 500 mg/kg or tiplaxtinin High dose at 5000 mg/kg). On day 28 mice were sacrificed and skin tissues prepared for histological analysis by Mason Trichrome stain. A) Bleomycin control chow (No Treatment), B) Bleomycin MDI-2517 chow, C) Bleomycin Tiplaxtinin Low dose chow, D) Bleomycin Tiplaxtinin High does chow, E) Quantification of skin thickness from Mason Trichrome stained slides. Data is shown as mean ± SD, n is indicated in each figure by the individual data points (10), scale bar = 100μm, ** $p<0.01$, *** $p<0.001$, by one-way ANOVA.

Figure 10, Lung trichrome staining from the comparator Study MDI-2517, Tiplaxtinin Low and High Dose. Twelve-week-old male C57BL/6J mice were subcutaneously implanted with osmotic pumps that deliver 100U/kg (total) of bleomycin over 7 days. The pumps were then removed, and at that time the mice were placed on treatment chows (drug concentration in chow: Vehicle, 0 mg/kg, MDI-2517 at 500 mg/kg, tiplaxtinin Low dose at 500 mg/kg or tiplaxtinin High dose at 5000 mg/kg). On day 28 mice were sacrificed and lung tissues prepared for histological analysis by Mason Trichrome stain. A) Bleomycin control chow (No Treatment), B) Bleomycin MDI-2517 chow, C) Bleomycin Tiplaxtinin Low dose chow, D) Bleomycin Tiplaxtinin High dose chow, E) Ashcroft Modified score of lung tissue from Mason Trichrome stained slides, F) Picrosirius Red quantification from Mason Trichrome stained slides. Data is shown as mean ± SD, n is indicated in each figure by the individual data points (7-10), scale bar = 35μm, ** $p<0.01$, *** $p<0.001$, **** $p<0.0001$ in panel E and F, by one-way ANOVA.

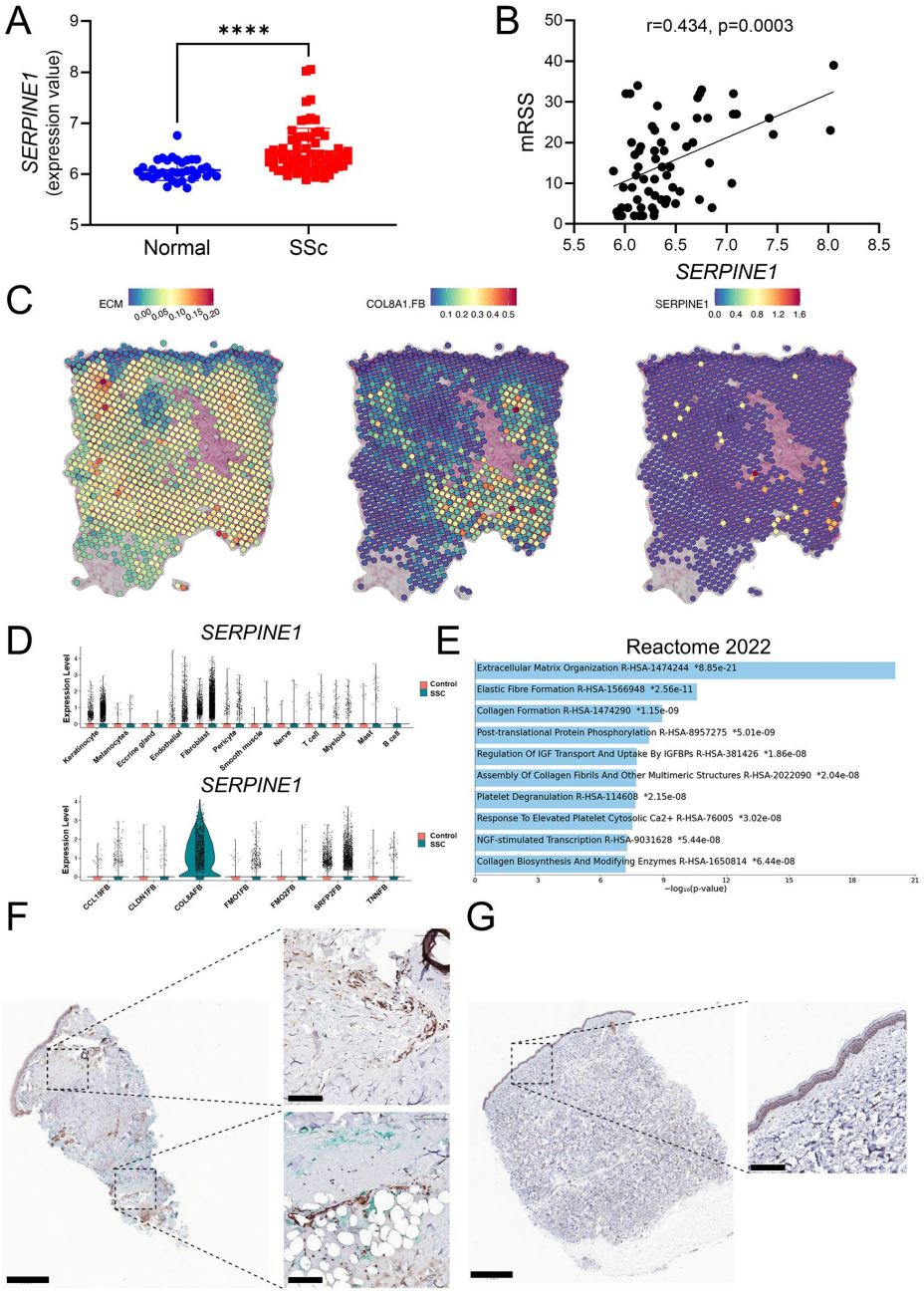

Figure 1. Expression of PAI-1 in SSc skin. A) Comparison of *SERPINE1* expression in SSc and healthy control skin biopsy samples from the GEO dataset (GSE58095). B) Correlation analysis of mRSS scores vs. *SERPINE1* expression from the data in A. C) Enriched signature for expression of extracellular matrix (ECM) genes along with expression of the myofibroblasts marker *COL8A1*, and *SERPINE1* (PAI-1) expression in SSc skin on the 10X Visium spatial platform (data representative of n=4). D) Violin plots of *SERPINE1* expression in controls vs. SSc skin across scRNA-seq data from different cellular populations (upper panel) and fibroblast subsets (lower panel). (n=18 healthy controls, n=22 SSc patients) E) Enriched biological processes in *SERPINE1*+ vs. *SERPINE1*- *COL8A1* myofibroblasts. F) IHC of PAI-1 in SSc skin biopsy (data representative of n=6). G) IHC of PAI-1 in skin biopsy from a healthy volunteer. Scale bar on overall biopsy is 500um, and 50um on the inserts. **** p<0.0001, by two tail Mann-Whitney test in panel A and p=0.0003 by Spearmann r correlation test in panel B.

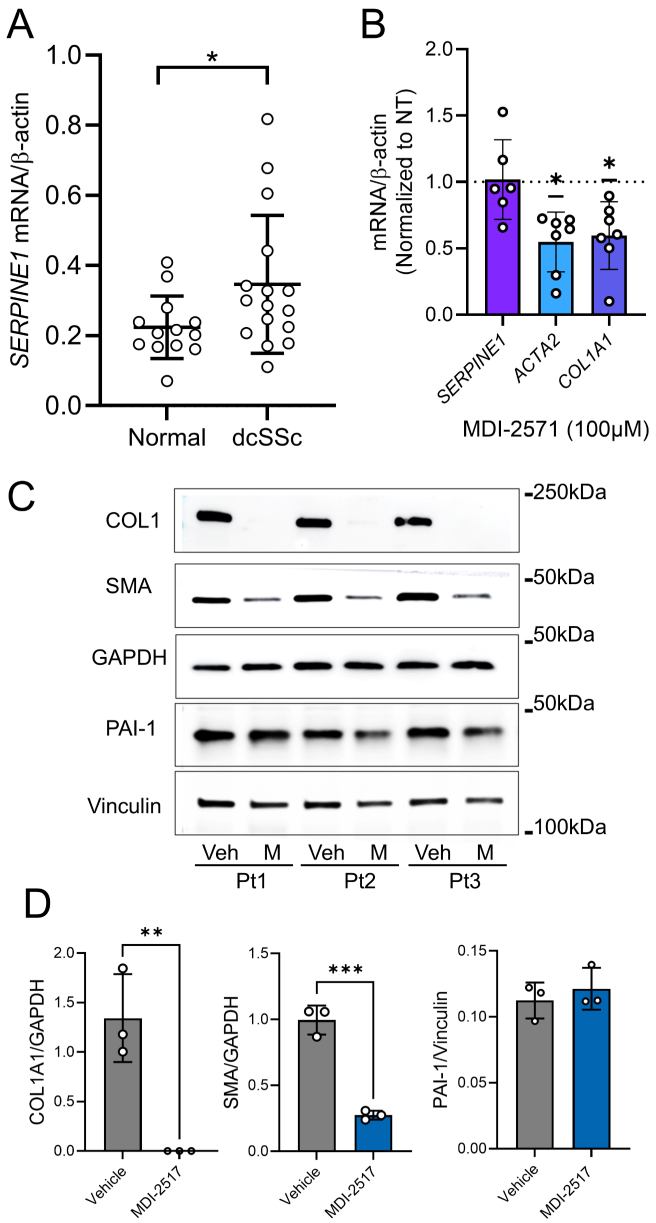

Figure 2. Downregulate pro-fibrotic markers in human SSc fibroblasts by MDI-2517. Dermal fibroblasts were isolated from punch biopsies from the distal forearm of healthy volunteers and diffuse cutaneous (dc)SSc patients. A) QPCR of PAI-1 (*SERPINE1*) mRNA expression in fibroblasts from normal skin and from SSc patients. B) Downregulate mRNA expression of pro-fibrotic markers, SMA and *COL1A1*, with MDI-2517 treatment. C) Western blot analysis shows reduction in COL1, SMA, and PAI-1 protein in SSc fibroblasts with and without MDI-2517 treatment. D) Quantification of the western blots in C, SMA and *COL1A1* are shown as the ratio to GAPDH and PAI-1 to vinculin. Data is shown as mean ± SD, n is indicated in each figure by the individual data points (3-17), * $p<0.05$, ** $p<0.01$, *** $p<0.001$, by two-tailed Mann-Whitney test in A, by a one sample Wilcoxon in B, and a two-tailed t test in D.

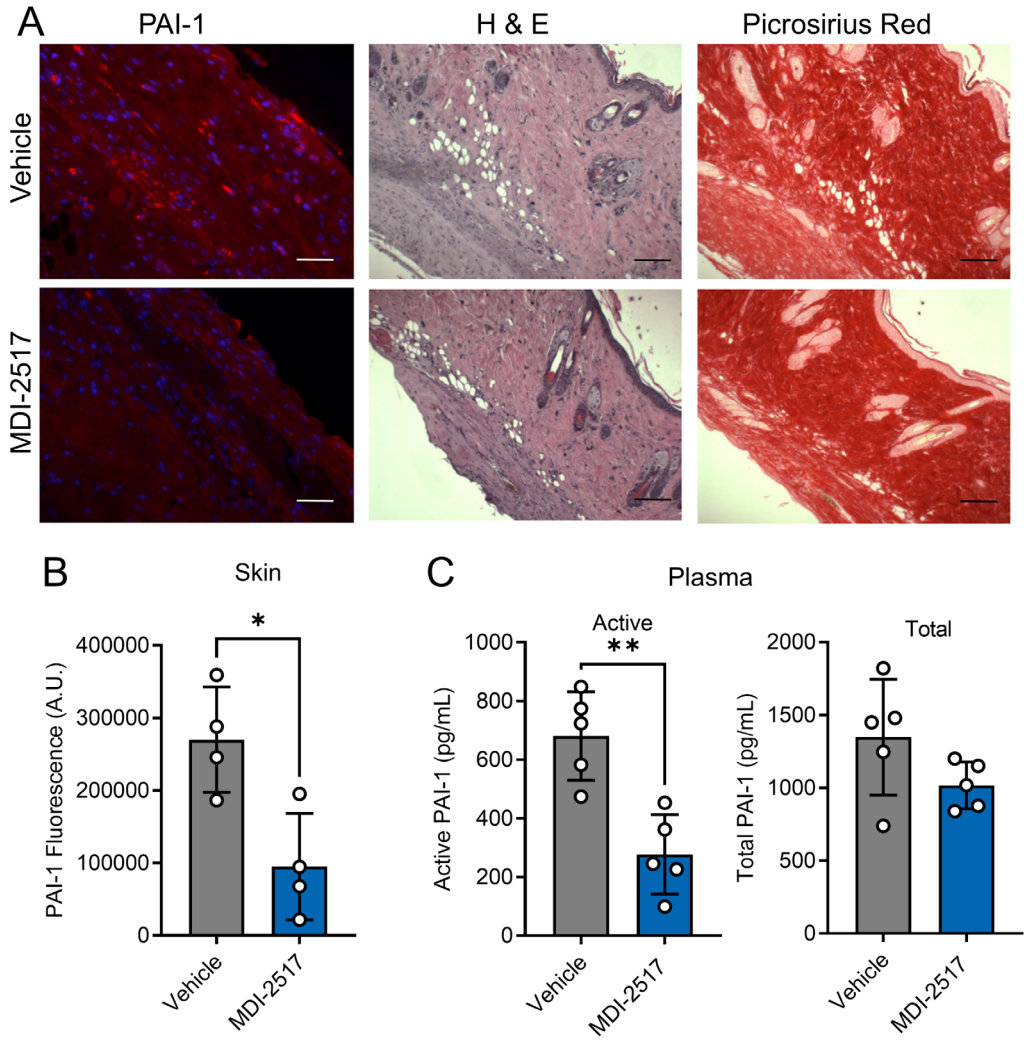

Figure 3. Target engagement of MDI-2517. Twelve-week-old male C57BL/6J mice were subcutaneously implanted with osmotic pumps that deliver 100U/kg (total) of bleomycin over 7 days. The pumps were then removed, and at that time the mice were placed on chow containing 0 mg/kg (Vehicle) or MDI-2517 at 500 mg/kg chow. On day 28 skin tissue and plasma and were collected. PAI-1 antigen in skin was quantified by immunofluorescence microscopy, images were acquired using the same settings and taken in comparable regions for each skin sample. For quantification 5 areas of interest per skin sample were analyzed (n=4 mice per treatment group) and the area of antibody immunoreactivity above a set threshold was measured and averaged for each animal using ImageJ. Panel A) Immunofluorescent staining of PAI-1 (red) and DAPI nuclear stain (blue), hematoxylin and eosin (H&E) and Picrosirius Red staining. Panel B) Quantification of the relative PAI-1 antigen in skin of the untreated and MDI-2517 treated mice. Panel C) Active and total PAI-1 in plasma. Data is shown as mean ± SD, n is indicated in each figure by the individual data points (4-5), scale bar = 100μm, * $p<0.05$ in panel B, ** $p<0.01$ in panel C, by two-tailed t-test.

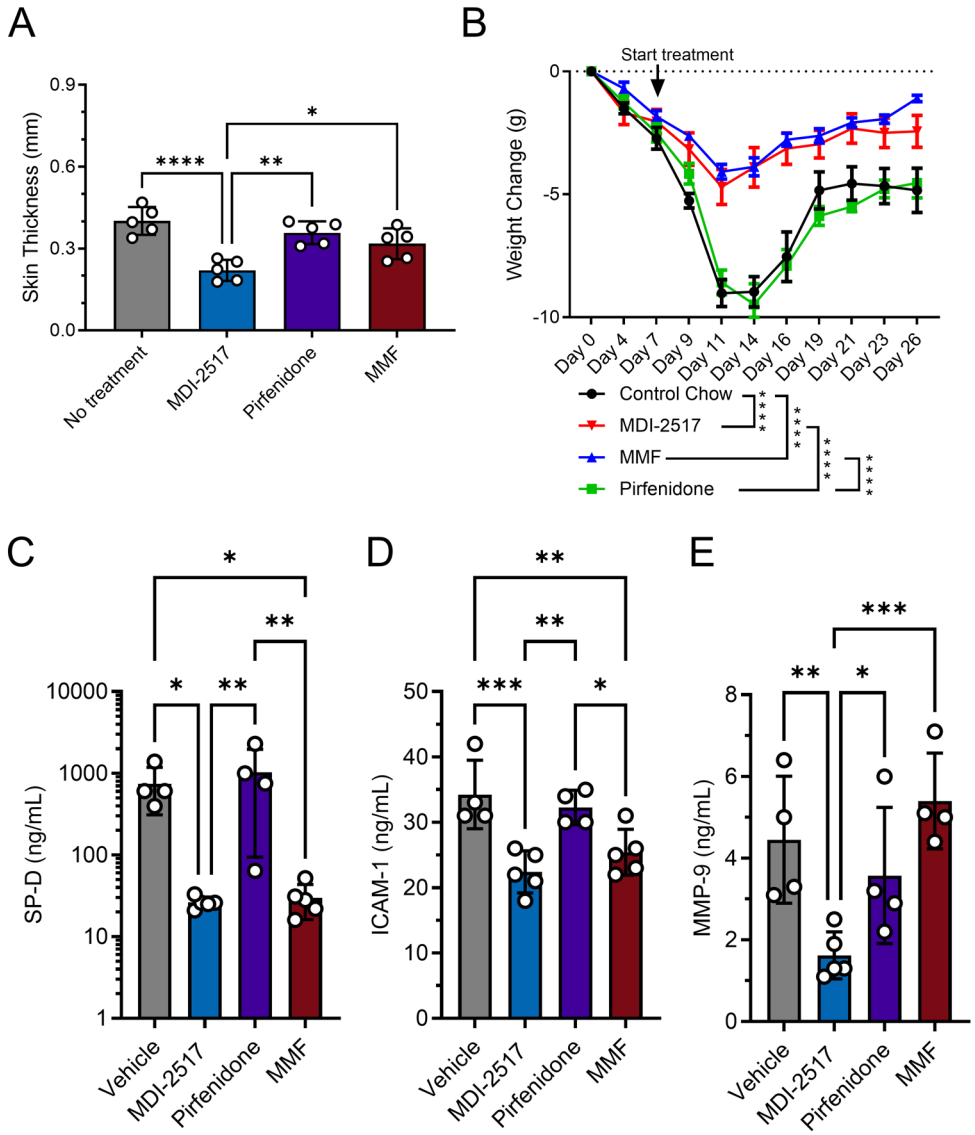

Figure 4. Comparator study of MDI-2517, pirfenidone and mycophenolate mofetil (MMF). Twelve-week-old male C57BL/6J mice were subcutaneously implanted with osmotic pumps that deliver 100U/kg (total) of bleomycin over 7 days. The pumps were then removed, and at that time the mice were placed on treatment chows (drug concentration in chow: Vehicle, 0mg/kg, MDI-2517 at 500mg/kg, pirfenidone at 1000mg/kg, MMF at 1000mg/kg). A) On day 28 skin thickness is determined at multiple locations by skin pinch with calipers then sacrificed and plasma and skin tissues collected. B) Body weight changes monitored approximately every 3 days. C-E) Biomarkers measured by antibody based Luminex multiplex assay. Data is shown as mean ± SD, n is indicated in each figure by the individual data points (4-5), * $p<0.05$, ** $p<0.01$, *** $p<0.001$, **** $p<0.0001$, by one-way ANOVA in panels A, C-E and by a repeated measures mixed-effect model in panel B.

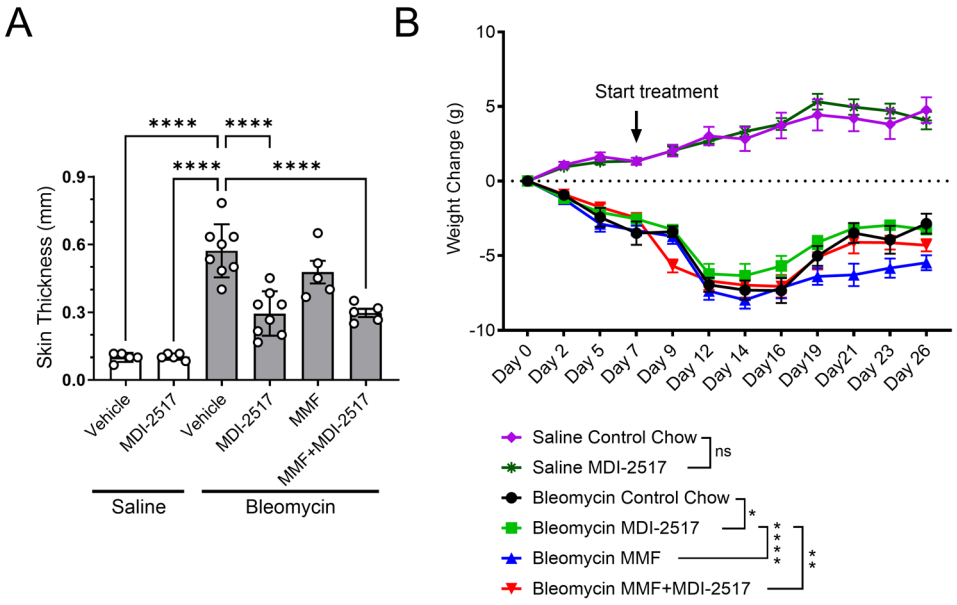

Figure 5, Comparator study of MDI-2517, mycophenolate (MMF) and MMF+MDI-2517. Twelve-week-old male C57BL/6J mice were subcutaneously implanted with osmotic pumps that deliver 100U/kg (total) of bleomycin over 7 days. The pumps were then removed, and at that time the mice were placed on treatment chows (drug concentration in chow: Vehicle, 0 mg/kg, MDI-2517 at 500 mg/kg, MMF at 1000mg/kg or combined MDI-2517 at 500 mg/kg and MMF at 1000 mg/kg,). A) On day 28 skin thickness was determined at multiple locations by skin pinch with calipers then sacrificed and tissues collected. B) Body weight changes monitored approximately every 3 days. Data is shown as mean ± SD, n is indicated in each figure by the individual data points (5-8), * $p<0.05$, ** $p<0.01$, **** $p<0.0001$, by one-way ANOVA in panel A and by a repeated measures mixed-effect model in panel B.

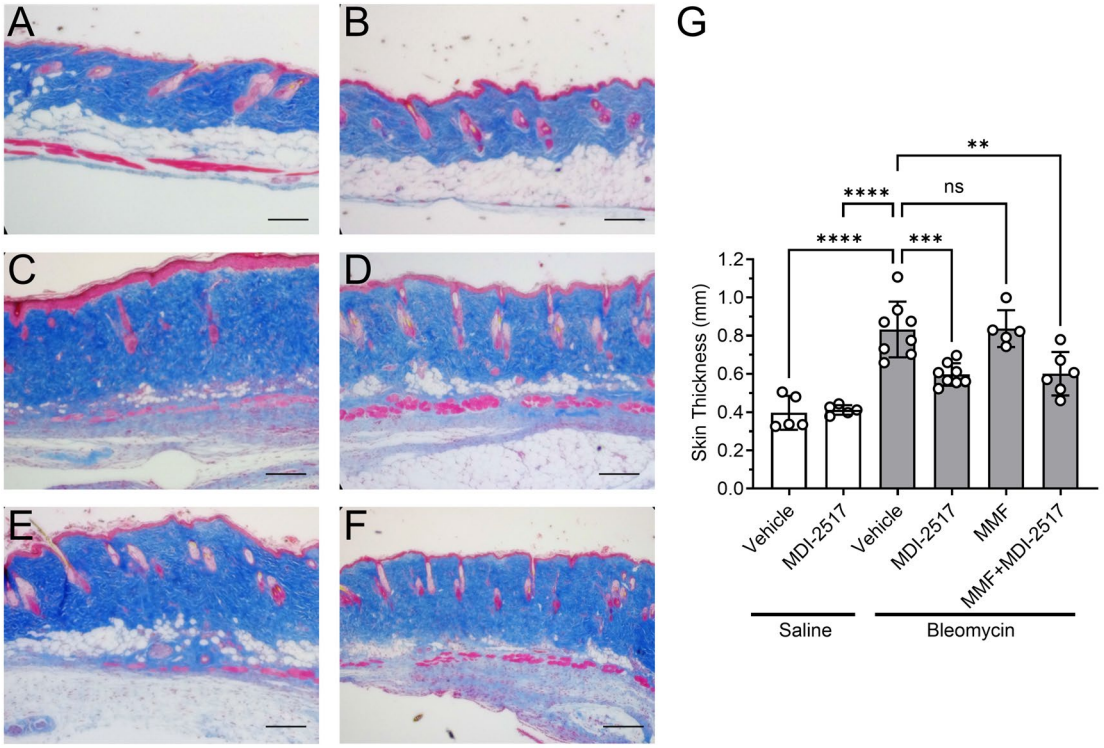

Figure 6, Skin trichrome staining from the comparator study of MDI-2517, mycophenolate (MMF) and combined MMF+MDI-2517. Twelve-week-old male C57BL/6J mice were subcutaneously implanted with osmotic pumps that deliver 100U/kg (total) of bleomycin or saline over 7 days. The pumps were then removed, and at that time the mice were placed on treatment chows (drug concentration in chow: Vehicle, 0 mg/kg, MDI-2517 at 500 mg/kg, MMF at 1000mg/kg or combined MDI-2517 at 500 mg/kg and MMF at 1000 mg/kg,). On day 28, skin tissues were prepared for histological analysis by Mason Trichrome Stain. A) Saline pump Control Chow, B) Saline pump MDI-2517 chow, C) Bleomycin control chow (No Treatment), D) Bleomycin MDI-2517 chow, E) Bleomycin MMF chow, F) Bleomycin combined MMF and MDI-2517 chow, G) Quantification of skin thickness from Mason Trichrome stained slides. Data is shown as mean ± SD, n is indicated in each figure by the individual data points (5-8), scale bar = 100μm, ** $p<0.01$, *** $p<0.001$, **** $p<0.0001$, by one-way ANOVA.

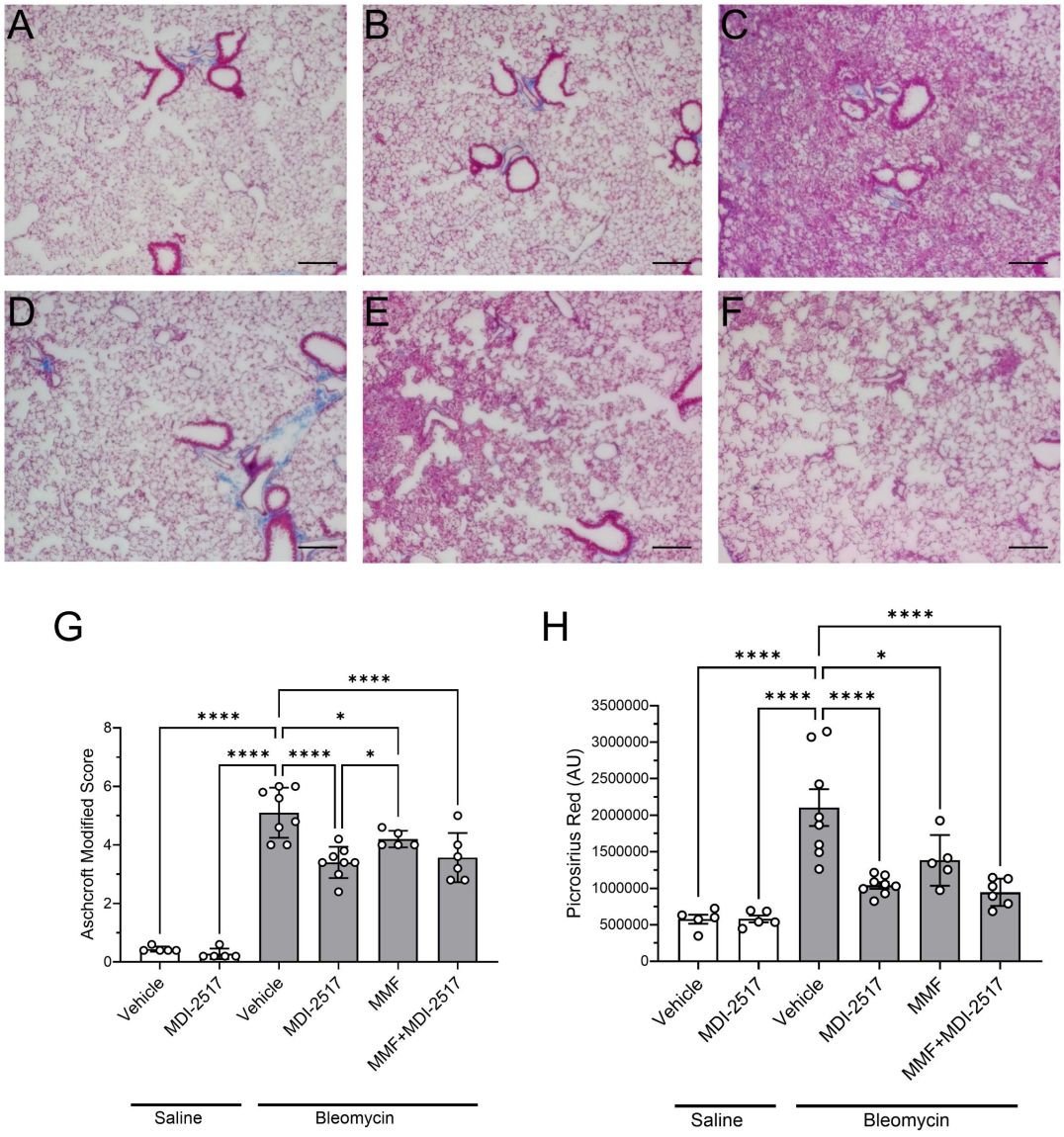

Figure 7, Lung trichrome staining from the comparator study of MDI-2517, mycophenolate (MMF) and combined MMF+MDI-2517. Twelve-week-old male C57BL/6J mice were implanted with osmotic pumps that deliver 100U/kg (total) of bleomycin or saline over 7 days. The pumps were then removed, and at that time the mice were placed on treatment chows (drug concentration in chow: Vehicle, 0 mg/kg, MDI-2517 at 500 mg/kg, MMF at 1000mg/kg or combined MDI-2517 at 500 mg/kg and MMF at 1000 mg/kg,). On day 28, lung tissues were prepared for histological analysis by Mason Trichrome stain and Picrosirius Red stain. A) Saline pump Control Chow, B) Saline pump MDI-2517 chow, C) Bleomycin control chow (No Treatment), D) Bleomycin MDI-2517 chow, E) Bleomycin MMF chow, F) Bleomycin combined MMF and MDI-2517 chow, G) Ashcroft Modified score of lung tissue from Mason Trichrome stained slides, H) Picrosirius Red quantification from stained slides. Data is shown as mean ± SD, n is indicated in each figure by the individual data points (5-8), scale bar = 35μm, * $p<0.05$, **** $p<0.0001$, by one-way ANOVA in panel G and H.

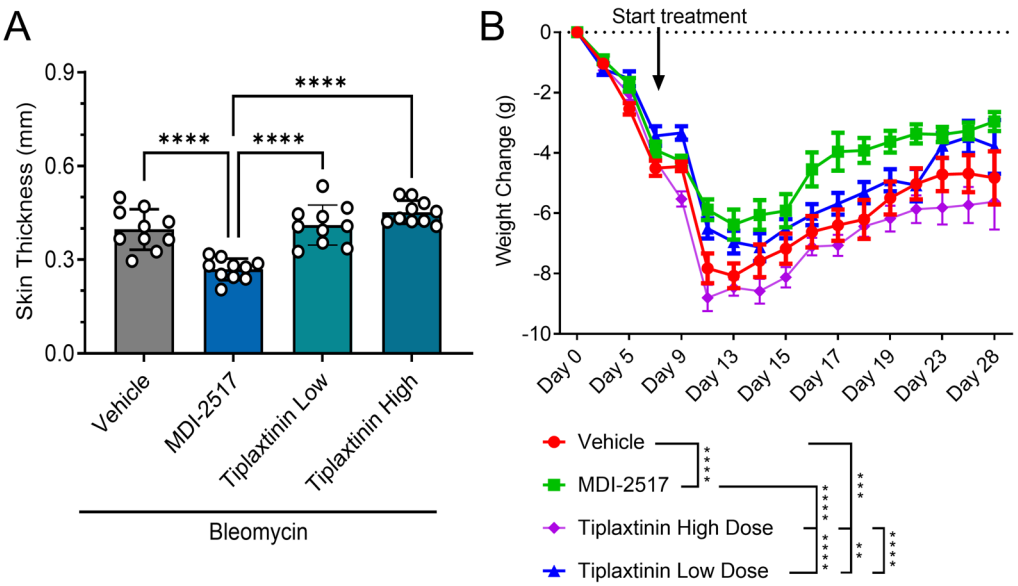

Figure 8, Comparator Study MDI-2517, Tiplaxtinin Low and High Dose. Twelve-week-old male C57BL/6J mice were subcutaneously implanted with osmotic pumps that deliver 100U/kg (total) of bleomycin over 7 days. The pumps were then removed, and at that time the mice were placed on treatment chows (drug concentration in chow: Vehicle, 0 mg/kg, MDI-2517 at 500 mg/kg, tiplaxtinin Low dose at 500 mg/kg or tiplaxtinin High dose at 5000 mg/kg). A) On day 28 skin thickness is determined at multiple locations by skin pinch with calipers then sacrificed and tissues collected. B) Body weight changes monitored approximately every 3 days. Data is shown as mean ± SD, n is indicated in each figure by the individual data points (10), ** p<0.01,*** p<0.001, **** p<0.0001, by one-way ANOVA in panel A and by a repeated measures mixed-effect model in panel B.

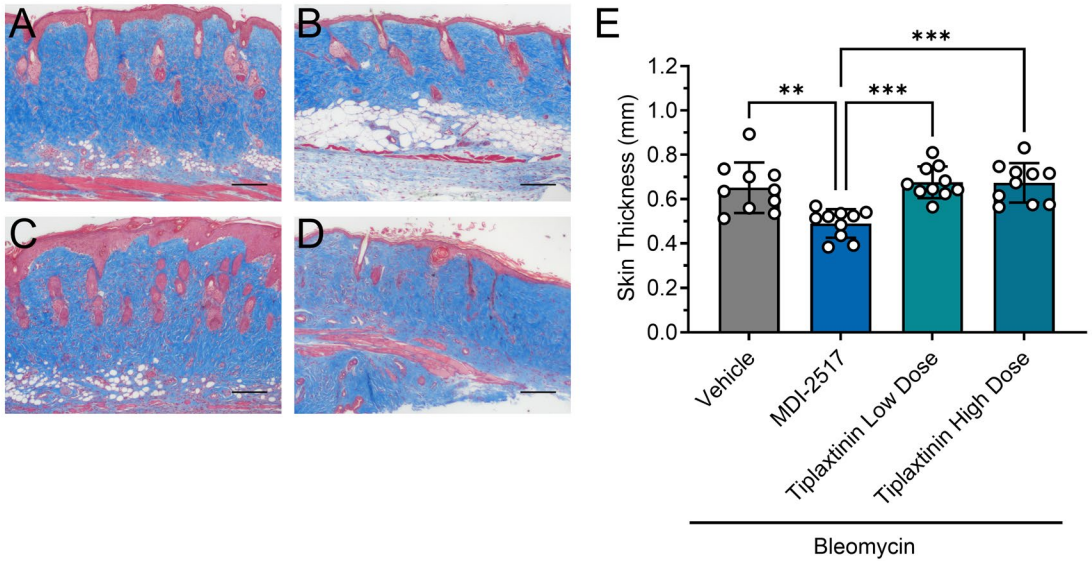

Figure 9, Skin thickness by Mason Trichrome from comparator Study MDI-2517, Tiplaxtinin Low and High Dose. Twelve-week-old male C57BL/6J mice were subcutaneously implanted with osmotic pumps that deliver 100U/kg (total) of bleomycin over 7 days. The pumps were then removed, and at that time the mice were placed on treatment chows (drug concentration in chow: Vehicle, 0 mg/kg, MDI-2517 at 500 mg/kg, tiplaxtinin Low dose at 500 mg/kg or tiplaxtinin High dose at 5000 mg/kg). On day 28 mice were sacrificed and skin tissues prepared for histological analysis by Mason Trichrome stain. A) Bleomycin control chow (No Treatment), B) Bleomycin MDI-2517 chow, C) Bleomycin Tiplaxtinin Low dose chow, D) Bleomycin Tiplaxtinin High does chow, E) Quantification of skin thickness from Mason Trichrome stained slides. Data is shown as mean ± SD, n is indicated in each figure by the individual data points (10), scale bar = 100μm, ** $p<0.01$, *** $p<0.001$, by one-way ANOVA.

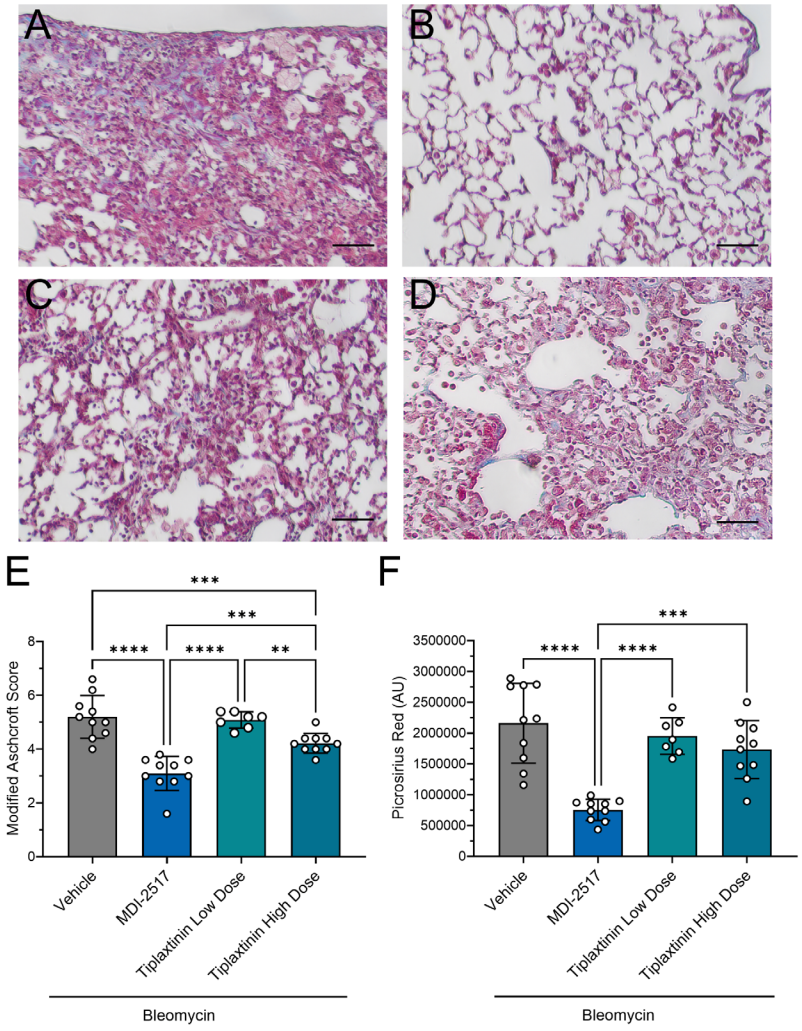

Figure 10, Lung trichrome staining from the comparator Study MDI-2517, Tiplaxtinin Low and High Dose. Twelve-week-old male C57BL/6J mice were subcutaneously implanted with osmotic pumps that deliver 100U/kg (total) of bleomycin over 7 days. The pumps were then removed, and at that time the mice were placed on treatment chows (drug concentration in chow: Vehicle, 0 mg/kg, MDI-2517 at 500 mg/kg, tiplaxtinin Low dose at 500 mg/kg or tiplaxtinin High dose at 5000 mg/kg). On day 28 mice were sacrificed and lung tissues prepared for histological analysis by Mason Trichrome stain. A) Bleomycin control chow (No Treatment), B) Bleomycin MDI-2517 chow, C) Bleomycin Tiplaxtinin Low dose chow, D) Bleomycin Tiplaxtinin High dose chow, E) Ashcroft Modified score of lung tissue from Mason Trichrome stained slides, F) Picrosirius Red quantification from Mason Trichrome stained slides. Data is shown as mean ± SD, n is indicated in each figure by the individual data points (7-10), scale bar = 35μm, ** p<0.01, *** p<0.001, **** p<0.0001 in panel E and F, by one-way ANOVA.